arXiv:2112.14688v2 [quant-ph] 12 Apr 2023

Preparing thermal states on noiseless and noisy programmable quantum processors

Oles Shtanko[1,*] and Ramis Movassagh[2,3,†]

[1]*IBM Quantum, IBM Research – Almaden, San Jose CA, 95120, USA*
[2]*IBM Quantum, MIT-IBM Watson AI lab, Cambridge MA, 02142, USA*
[3]*Google Quantum AI, Venice Beach, CA 90291, USA*

Nature is governed by precise physical laws, which can inspire the discovery of new computer-run simulation algorithms. Thermal states are the most ubiquitous for they are the equilibrium states of matter. Simulating thermal states of quantum matter has applications ranging from quantum machine learning to better understanding of high-temperature superconductivity and quantum chemistry. The computational complexity of this task is hopelessly hard for classical computers [1]. The existing quantum algorithms come with caveats: most either require quantum phase estimation [2–5] rendering them impractical for current noisy hardware, or are variational [6–8] which face obstacles such as initialization, barren plateaus, and a general lack of provable guarantee [9]. We provide two quantum algorithms with provable guarantees to prepare thermal states on (near-term) quantum computers that avoid these drawbacks. The first algorithm is inspired by the natural thermalization process where the ancilla qubits act as the infinite thermal bath. This algorithm can potentially run in polynomial time to sample thermal distributions of ergodic systems– the vast class of physical systems that equilibrate in isolation with respect to local observables. The second algorithm works for any system and in general runs in exponential time. However, it requires significantly smaller quantum resources than previous such algorithms. In addition, we provide an error mitigation technique for both algorithms to fight back decoherence, which enables us to run our algorithms on the near-term quantum devices. To illustration, we simulate the thermal state of the hardcore Bose-Hubbard model on the latest generation of available quantum computers.

Nature has inspired many modern classical algorithms [10]. Here, we propose a new algorithm inspired by natural equilibration that is designed to prepare Gibbs states on quantum hardware.

Gibbs states are fundamental as they represent the natural equilibrium state of many-body systems in physics and chemistry. Simulating Gibbs distributions on a quantum hardware offers an opportunity to explore equilibrium many-body phenomena [11], including strongly-correlated quantum matter [12] and high-energy physics [13]. The quantum simulation of Gibbs states would enable accurate predictions of molecular structures and reaction rates [14]. As such, it provides a significant advantage over classical ones as they suffer from the infamous sign problem [1]. The Gibbs states are used in computer science and quantum computing as well. For example, the low-temperature Gibbs states provide an approximation to optimization problems by encoding them into the lowest energy states [15]. In quantum machine learning, Gibbs distribution can be used to create generative models that are superior to classical counterparts [16]. Finally, for systems with sufficiently large energy gap between the smallest two energies (so-called finite energy gap), preparation of Gibbs states may recover the quantum information encoded in the ground state [17]. Thus, there is an active frontier for developing heuristic methods to simulate thermalization tailored to different experimental platforms [18–24].

Preparation of generic Gibbs states is a challenging task from the standpoint of computational complexity. For classical systems, sampling from the Gibbs state is a NP-hard problem. In the quantum case, this problem is believed to be even harder and be complete in the formidable complexity class known as quantum Merlin Arthur (QMA) [25–29], which is the analog of NP for quantum computers. It is therefore unlikely that an efficient algorithm can be found that is applicable to all quantum systems. In fact algorithms with provable performance [2, 3, 30, 31] have convergence times that scale exponentially with the system size. However, some empirical algorithms, such as the quantum Metropolis algorithm [4, 5, 32], can succeed in polynomial time for certain systems.

A formal implementation of quantum MH algorithm utilizes non-local operations as well as the quantum phase estimation subroutine, which is resource-intensive and very sensitive to noise rendering it impractical especially in the near-term. Despite recent progress in hardware-efficient algorithms that use only local gates and designed for low-correlated systems [33, 34], there is push for constructing Gibbs states for more general classes of systems.

The quantum dynamics of an isolated system is generated by its Hamiltonian. Given the target Hamiltonian H, the goal is to obtain samples from the mixed state

$$\rho_\beta = \frac{1}{Z_\beta}\exp(-\beta H), \quad Z_\beta = \mathrm{Tr}\left[\exp(-\beta H)\right], \qquad (1)$$

where β is inverse temperature and Z_β is a partition function. This state is the fixed point of the evolution of the system in contact with a much larger (hypothetically in-

* oles.shtanko@ibm.com
† movassagh@google.com

finite) reservoir at inverse temperature β.

In this paper, we present two algorithms for preparing the Gibbs state on the quantum computer that avoid the quantum phase estimation subroutine. The first algorithm is inspired by the natural thermalization process where the ancilla qubits act as the infinite thermal bath [20, 35, 36]. This algorithm can potentially run in polynomial time to sample thermal distributions of ergodic systems– the vast class of physical systems that equilibrate in isolation with respect to local observables. The second algorithm works for any system and in general runs in exponential time. However, it requires significantly smaller quantum resources than previous such algorithms. Both algorithms can be run on the near-term noisy quantum computers as we will demonstrate below.

Our algorithms have the advantage of utilizing random local quantum circuits, which by definition are not fine-tuned. Motivated by the challenges of the near-term quantum computation era in which effects of noise and decoherence cannot yet be corrected, we find that treating the random parameters in the circuits as adjustable leads to substantial mitigation of errors caused by decoherence and noise. The adjustment of parameters resembles that of the variational algorithms [6–8]. However, in this work the optimization over the parameters only serves to reduce the effects of noise. Consequently, the algorithms do not suffer as much from the problem of barren plateaus [9].

Quantum Ergodicity. In Nature one encounters two major classes of physical systems that in some ways are at extremes. These are integrable and chaotic systems.

Integrable systems are often idealizations constrained by symmetries, transition rules, and integrals of motion. They may allow for exact analytical solutions such as those obtained by the Yang-Baxter equations or Bethe-Ansatz. Chaotic systems on the other hand lack the fine tuning necessary for integrability. These include most interacting systems in presence of weak disorder. Chaotic systems derive significance from the fact that the behavior of weakly perturbed models are well-approximated by chaotic behavior at sufficiently high temperatures.

The dynamics of chaotic systems are ergodic, which means they are only constrained by energy conservation. A key feature of ergodic systems is that their local observables usually quickly reach their thermal equilibrium values. Calculating these thermal values is often challenging for traditional analytical or numerical methods. However, as we will show, it is possible to use quantum computers to generate quantum states that accurately describe the thermal state of an ergodic system. The behavior of an ergodic system is commonly described by ETH which are certain conditions on the eigenstates $|\mu\rangle$ of the Hamiltonian of the system [37–41, 59].

Mathematically, ETH's premise is that for any *local* operator V and any two eigenstates $|\mu\rangle$ and $|\nu\rangle$ within a certain energy interval, the matrix elements $\langle\mu|V|\nu\rangle$ satisfy $\langle\mu|V|\nu\rangle = v_\mu\delta_{\mu\nu} + e^{-O(n)}R_{\mu\nu}$, where v_μ are real

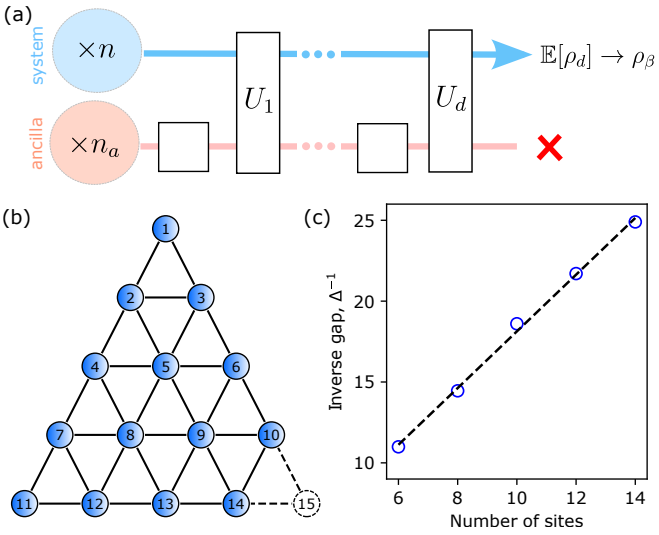


FIG. 1. **Ergodic algorithm and its performance** (a) Illustration of the ergodic algorithm. The qubits are divided into two parts, a system of n qubits and an ancilla of n_a qubits. The ancilla is reset to a thermal state at the beginning of each cycle; during the cycle both parts are weakly coupled by the Hamiltonian in Eq. (2). (b) The layout of a lattice half-filled with hardcore bosons obeying the Hamiltonian in Eq. (7) with $J = 1$ and $U = 0.1$. The circles represent the sites that can be occupied by a single boson, the edges connect the nearest neighbors. (c) The inverse gap Δ^{-1} of the underlying classical Markov process in our algorithm (Theorem 1) for the system in (b) with $\beta = 1$, $\Omega = 1$, and $\gamma = 0.1$. The inverse gap grows linearly with the system size of the truncated system (as shown by the dashed line), where the truncation is performed in numerical order (i.e., a system of n sites includes the sites $1, \ldots, n$).

numbers, $n \gg 1$ is the number of qubits, and $R_{\mu\nu}$ are standard Gaussian variables. In words, ETH says that the off-diagonal elements are random and exponentially small in n. This property has been numerically verified for a wide range of physical systems [40–42].

Our ergodic algorithm described just below gives rigorous guarantees for the preperation of the thermal state on a quantum computer for systems that obey the ETH. We leave the question of the performance of this algorithm for more general Hamiltonians for future work. We will show that the infinite reservoir is mimicked by a finite number of independent, properly reset and randomized ancilla-qubits, that are weakly coupled to the system. The ancilla qubits extract entropy from the system qubits in the course of the quantum computation, whereby thermalize the system-qubits at inverse temperature β. This essentially a quantum circuit adaption of the textbook concept of bringing the system in contact with an infinite reservoir, where the reservoir is played by the ancilla qubits.

Ergodic algorithm. The summary of the algorithm is as follows. First, we assign n qubits to be the "system"

qubits on which the target Hamiltonian H acts. We initialize these to a random product state. We then pick n_a "ancilla" qubits and initialize each to $|0\rangle$. The algorithm consists of d cycles (Fig. 1a). At the beginning of each cycle, the "ancilla" qubits are reset to $|0\rangle$ and then each is easily put in a single-qubit thermal equilibrium state of an assigned random single-qubit Hamiltonian. Throughout the cycle, all the qubits evolve under combined Hamiltonians of the ancilla and the system with a weak coupling between them (see Fig. 1b). The evolution time at the kth cycle, t_k, is random from the exponential distribution $\gamma \exp(-\gamma t_k)$, and is generated by the Hamiltonian

$$\mathcal{H}_k = H \otimes I_{\text{anc}} + I_{\text{sys}} \otimes H^k_{\text{anc}} + \lambda \sum_{m=1}^{n_a} V_{km} \otimes X_m, \quad (2)$$

where V_{km} are ℓ-local random operators acting on the system qubits, $H^k_{\text{anc}} = \frac{1}{2}\sum_{m=1}^{n_a} \omega_{km} Z_m$ is a one-local Hamiltonian on the ancilla qubits, X_m and Z_m are a Pauli-X and Z on the mth ancilla qubit, $\omega_{km} \in [-\Omega, \Omega]$ is uniformly random, and λ is the strength of the coupling. The process runs in time of $t = d/\gamma$ on average, where d is the total number of cycles.

We consider the regime where the parameters λ and γ are sufficiently small to allow for a weak coupling between the system and the ancilla. In this case, the expected density matrix is well described by a classical update rule given by a transition matrix T for a choice of parameters. Thus, we bridge the quantum problem to the classical Markov process. The convergence of the process depends on the gap Δ, i.e. the difference between the two largest eigenvalues of the corresponding matrix T. Under the above choice of parameters λ, γ, we obtain our main theorem (see Theorem S1 in Supplementary Information for a formal statement):

Theorem 1 *Given an inverse temperature β, and the error tolerance $0 < \epsilon \leq 1$, the expected output of the circuit $\mathbb{E}[\rho_d]$ becomes $\epsilon-$close to the true Gibbs state,*

$$\|\mathbb{E}[\rho_d] - \rho_\beta\|_1 \leq \epsilon,$$

in time $t = \tilde{O}(\beta m^3/\epsilon^2)$, where $m \leq O(n/\Delta)$ is a mixing time of the corresponding Markov process.

Here $\tilde{O}$ hides poly-log factors. We note that $O(n/\Delta)$ is only an upper-bound on the mixing time, and the algorithm may run faster than $t = \tilde{O}(\beta n^3/\Delta^3\epsilon^2)$.

From this result we can conclude that if Δ is polynomially small in the system size, the algorithm converges in polynomial time as well. As an example, we analyze the gap for a finite ergodic system of hardcore bosons (see details of the Hamiltonian below). For sizes up to 14 sites, this system exhibits a reasonable linear scaling of the inverse gap Δ^{-1} with the size of the system (Fig. 1c). A comparison of this algorithm to the well-known quantum Metropolis algorithm [4] can be found in the Supplementary Section I F. The resource estimation for this algorithm is shown in section I G.

Even though ergodic systems are common in nature, one may require a method for preparing Gibbs states for *general* Hamiltonians. Unlike in the ergodic setting, by to the QMA-hardness of Gibbs sampling for general Hamiltonians [25–29], it is expected that the scaling of the run-time for a universal algorithm would be exponential. Our second algorithm utilizes monitored random quantum circuits to prepare the Gibbs state. Random quantum circuits are also the backbone of models of quantum chaos [43], dynamic quantum phases [44], and modern quantum complexity theory [45–47]. We will show that any realization of our random circuit is likely a good Gibbs sampler, whereas averaging over circuits provides significant improvement compared to individual realizations.

Universal algorithm. In simple terms, this algorithm can be understood as applying an effective imaginary-time evolution operator $V_\beta \propto e^{-\beta H/2}$. Consider starting from a random initial state in the computational basis $|\mathbf{z}\rangle = |z_1 \dots z_n\rangle$, where $z_i \in \{0, 1\}$. Then the average over the initial state density matrix after the imaginary-time evolution is

$$\mathbb{E}_{\mathbf{z}} V_\beta |\mathbf{z}\rangle\langle\mathbf{z}| V_\beta^\dagger \propto \exp(-\beta H) \propto \rho_\beta. \quad (3)$$

To implement this operation, we construct a circuit that utilizes ancilla and intermediate measurements [31, 48].

For simplicity, consider Hamiltonians of the form $H = \sum_{m=1}^{M} h_m$, where $h_m \geq 0$ are positive local terms. Given a depth d, we define a small imaginary-time step $\delta\beta = \beta/d$, and the set of angles $\theta_{mk} \in \mathcal{N}(0, 1)$ to be standard normals. For each cycle k and term h_m we initialize an ancilla qubit to $|0\rangle$, and apply the gate

$$U(\theta_{mk}, h_m) = \exp(i\theta_{mk}\sqrt{\delta\beta h_m} \otimes X) \quad (4)$$

to the system qubits in the support of h_m and the ancilla qubit, where X is a Pauli-X acting on the ancilla. We then measure the corresponding ancilla qubit. At the end, we accept the output of the circuit only if all of the ancilla qubits evaluate to 0, otherwise we re-run the circuit. This is the source of exponential slow-down mentioned above. A gaussian integration reveals that the average over θ_{mk} results in each gate essentially enacting a short imaginary time evolution for h_m. Therefore, the overall imaginary time of evolution, β, is composed from such gates in a trotterized manner [49] in d cycles. Fig. 1(b) shows an example of the kth cycle.

The following theorem quantifies the convergence of the output ρ_{out} to the Gibbs state:

Theorem 2 *Let $\xi := \beta^2 M/d \ll 1$. Then for any $0 < \epsilon \leq 1$, the output after d cycles satisfies*

$$S(\rho_\beta \,\|\, \mathbb{E}[\rho_{\text{out}}]) \leq A\xi^2\,, \quad (5)$$

$$\text{Prob}\Big(S(\rho_\beta \,\|\, \rho_{\text{out}}) \geq \frac{\xi C}{\epsilon}\Big) \leq \epsilon, \quad (6)$$

where $S(\rho\|\sigma)$ is the relative entropy, and A and C are constants depending on h_m.

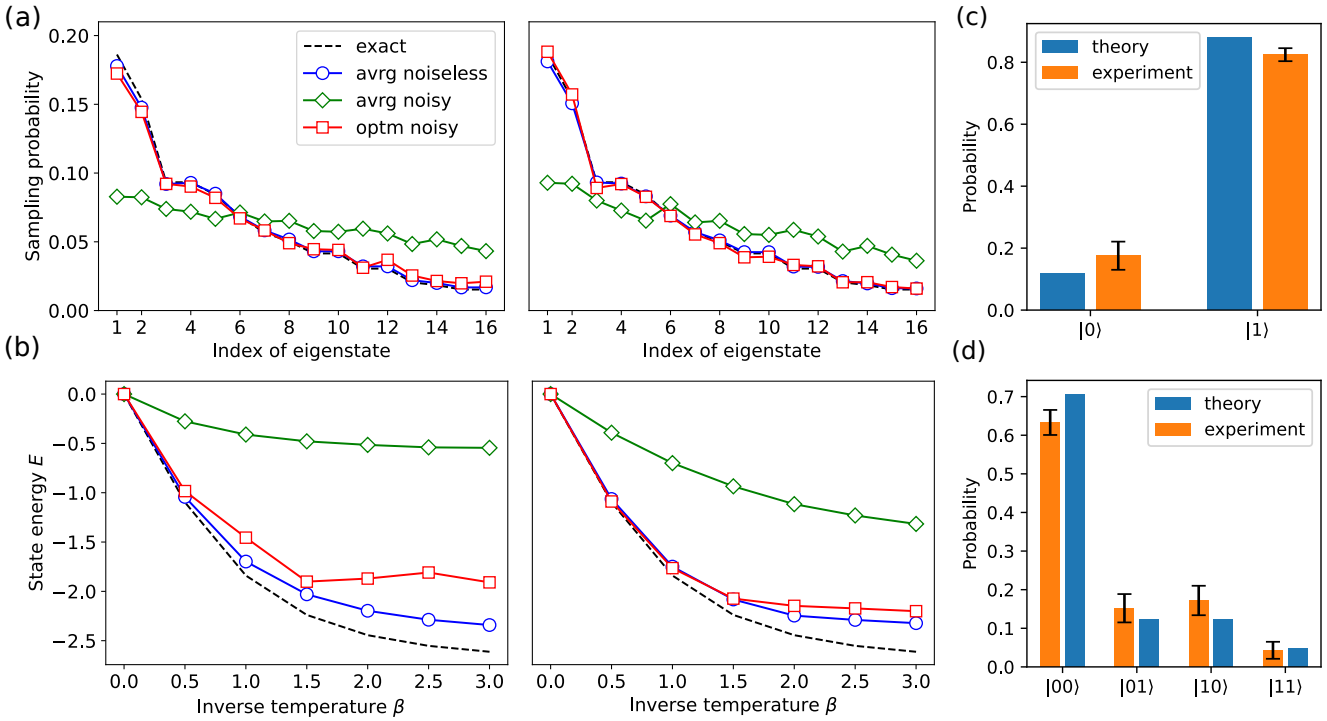


FIG. 2. **Simulations and experiments.** (a) and (b). Numerical simulations of a seven-qubit device including $n = 4$ one-dimensional system qubits and $n_a = 3$ ancilla qubits for the target Hamiltonian in Eq. (7), where $J = U = 1$. Panel (a) shows the probabilities of sampling Hamiltonian eigenstates for ergodic algorithm (left) and universal algorithm (right). The curves describe the $\beta = 1$ output averaged over 10^3 samples for: noiseless circuits (blue circles), noisy circuits (green diamonds), and noise-optimized circuits (red squares). Dashed lines show the exact solution. The number of cycles in the Ergodic algorithm is $d = 20$, $\gamma = 0.1$, and noise is modeled by single-qubit depolarizing channels after each cycle with the probability $p = \Gamma t$, where t is the cycle time and $\Gamma = 10^{-3}$ is the noise rate. In the universal algorithm, we take $d = 5$ cycles and take depolarizing noise which affects each qubit with probability $p = 10^{-2}$ after 2-qubit gates and $p' = 2 \cdot 10^{-2}$ after 3-qubit gates (see Supplementary Section II G for justification). (b) The expected energy of the output as the function of temperature in the same setting. (c) and (d) Implementation on IBM 7-qubit *ibm_casablanca* device. Histograms show the experimental sampling probabilities compared with the theoretical predictions. (c) Implementation of the ergodic algorithm for $n = 1$ system qubit and $n_a = 1$ ancilla qubit for Hamiltonian $H = Z_1$. The coupling is $\lambda = 0.1$ for the first cycle and it decreases linearly with number of cycles, inverse average time is $\gamma = 0.01$. Experiment uses 150 random circuit configurations with 8192 samples per circuit. (d) Sampling probabilities for the universal algorithm utilizing $n_a = 3$ ancilla qubits and $n = 2$ system qubits with the Hamiltonian $H = X_1X_2 - Z_1 - Z_2$. In the experiment we took 100 random circuit configurations with 8192 samples per circuit.

The probability and expectation in this theorem are taken with respect to the distribution of random angles θ_{mk} and ρ_{out} is output of a successful circuit run (i.e., where all ancilla measurements return 0).

To illustrate, let us assume that $\|h_m\| \leq O(1)$ and $M \propto n$, where n is the number of qubits as before. Then, in order to achieve $S(\sigma\|\rho) \leq \epsilon$ for a fixed error $\epsilon > 0$, the minimal required circuit depth is $d \propto O(n\beta^2/\sqrt{\epsilon})$ for the averaged result in Eq. (5), while a typical circuit requires depth $d \propto O(n\beta^2/\epsilon)$ according to Eq. (6). The acceptance probability for a large-d circuit is $p \simeq 2^{-n}\mathcal{Z}_\beta = 2^{-\alpha n}$, where $\alpha = 1 - (\log_2 \mathcal{Z}_\beta)/n$, therefore the algorithm time $t \propto 1/p$ grows exponentially with the number of qubits.

Due to the QMA-hardness of Gibbs sampling Hamiltonians, it is unlikely that this scaling can be improved without restrictions on the Hamiltonian. We detail the resource estimation for this algorithm in the Supplementary Section II E. Despite exponential scaling of the performance time, this algorithm provides sufficient improvement over comparable algorithms targeted general Hamiltonians [2, 3, 30, 31].

We would like to remark on the utility of this algorithm when the terms h_m are proportional to local Pauli operators. Then, for the single-qubit terms, the gate in Eq. (4) can be implemented using only a single CNOT gate, compared to three CNOTs required for generic two-qubit gate [50]. Moreover, a gate corresponding to a two system-qubits term involves the total of three qubits. This in our algorithm requires only two CNOTs, and is much less than what is required for a general three-qubit gate (see Supplementary Section II G for details).

Demonstration. We illustrate our algorithm for the hardcore Bose-Hubbard model, which is often used to study strong interactions in quantum many-body systems. The Hamiltonian of this model is

$$H = -J \sum_{\langle i,j \rangle} (a_i^\dagger a_j + a_j^\dagger a_i) + U \sum_{\langle i,j \rangle} n_i n_j, \qquad (7)$$

where a_i are hard-core boson Fock operators satisfying $[a_j, a_j^\dagger] = 0$ for all $i \neq j$ and $\{a_i, a_i^\dagger\} = 1$ at the same site, $n_i = a_i^\dagger a_i$ are density operators, J is the hopping coefficient, U is the density-density coupling, and $\langle i, j \rangle$ denotes the sum over nearest sites. This model can be mapped onto a qubit spin system (see Supplementary Section III). The numerical behavior of the gap shown in Fig. 1c and the Theorem 1 together would imply that one can prepare the Gibbs state of this model on a quantum computer to the statistical distance ϵ in time $t = O(\beta n^6/\epsilon^2)$.

As a test of the algorithms in realistic setting, we compare the probability of sampling Hamiltonian eigenstates for a noisy and noiseless limited-depth algorithms with corresponding Gibbs distribution, see Fig. 2 (a) and (b). In particular, the system is not exactly ergodic for these sizes, yet the algorithm successfully approximates Gibbs states. Also, numerical simulations provide evidence that the noise degrades the accuracy of the output distribution, but does not completely destroy the result in small systems. Another method of measuring the accuracy of the algorithm is comparison of the temperature dependency of the output state energy $E = \mathbb{E}\mathrm{Tr}\,(\rho_{\mathrm{out}} H)$ with the exact values $E_\beta = \mathrm{Tr}\,(\rho_\beta H)$. This comparison is shown in bottom panel of Fig. 2 (a) and (b). As we analytically predicted above, the algorithm better performs at higher temperatures $\beta \ll J, U$. We also implement the algorithms on the latest version of IBM quantum hardware, as shown in Fig 2 (c) and (d).

Error mitigation. Decoherence caused by noise is a major limitation for the current generation of quantum hardware. In addition to existing error mitigation techniques, here we show that both of our algorithms allow for a complementary way of error mitigation. We note that circuits in both algorithms depend on multiple random parameters. The choice of these parameters is mostly irrelevant in the ideal setting of zero noise and unlimited depth. Numerical results below show that, in a realistic setting, certain choices of parameters lead to a better performance, by reducing the effect of noise. The result can be optimized over these parameters in order to significantly improve the results.

In order to improve the output of a noisy circuit, we take as the objective function the free energy of the output, and try to minimize it by adjusting the parameters in the model. We do not take into account the complexity of measuring free energy and leave it for future work. We find that such an optimization significantly reduces the effect of depolarizing noise, see Fig. 2 (a) and (b).

Discussions. We provide two algorithms for sampling from the Gibbs distributions of quantum Hamiltonians. The first assumes ergodic Hamiltonians that obey the ETH hypothesis, and the second is universal. In the first case, we obtain a quantum algorithm that is implemented on a quantum circuit with local architecture whose complexity is similar to the quantum Metropolis-Hastings algorithms but does *not* require the quantum phase estimation subroutine. Our second algorithm can also be implemented on a quantum circuit and is in general an exponential time algorithm as expected. We demonstrated both algorithms on actual near-term quantum hardware. In addition, we found a way to mitigate errors in both algorithms by running an optimization routine over the parameter space that define the gates of the circuits. We find that our error mitigation technique is quite effective and in some cases reduces the effect of noise almost completely. Although, in general, error mitigation seems to require exponential samples [51], it remains an open problem whether for classes of Hamiltonians such as those obeying ETH more sample-efficient mitigation techniques exist.

Together with ours a recent simultaneous progress appeared [52]. Our result for the ergodic algorithm can be combined with this recent work to show that the QMH algorithms converge to the Gibbs state in a polynomial time for ETH systems [53]. This implies that ours is also a polynomial time algorithm. A further interesting aspect of the ergodic algorithm is the investigation of its applicability to non-equilibrium states of matter realized by Floquet Hamiltonians [54, 55].

A major open problem that is substantiated with our empirical explorations is to prove our first algorithm without the ETH assumption and for a more general class of Hamiltonians.

Another interesting open problem is to use our techniques to prove the cooling rate into the ground state. One can envisage ancilla being prepared in their ground state and derive convergence to the ground state of the system Hamiltonian such as those discussed in [36].

The geometrical locality of Hamiltonians can also be used to improve the precision of the universal algorithm. It is possible, for example, to reduce the resources required for low-dimensional Hamiltonians using the techniques proposed in [30]. Furthermore, the error can be reduced by using higher-order product formulas [56] and randomized gate positions [57]. For both algorithms, error mitigation can be improved by an optimization procedure that runs conditionally from layer to layer [58], as well as, other techniques in machine learning and in particular supervised machine learning.

Available Code. The code used to generate presented data is available at:
https://github.com/IBM/gibbs-qalgrthms/tree/latest

Acknowledgements. – We would like to thank David

Layden, Sarah Sheldon, Mario Motta, Jeff Cohn, Kunal Sharma, Abhinav Deshpande, and Kristan Temme for helpful discussions. We acknowledge funding from the MIT-IBM Watson AI Lab under the project *Machine Learning in Hilbert space*. The research was partly supported by the IBM Research Frontiers Institute.

[1] E. Y. Loh, J. E. Gubernatis, R. T. Scalettar, S. R. White, D. J. Scalapino, and R. L. Sugar, Sign problem in the numerical simulation of many-electron systems, Phys. Rev. B **41**, 9301 (1990).
[2] D. Poulin and P. Wocjan, Sampling from the thermal quantum gibbs state and evaluating partition functions with a quantum computer, Phys. Rev. Lett. **103**, 220502 (2009).
[3] A. Riera, C. Gogolin, and J. Eisert, Thermalization in nature and on a quantum computer, Phys. Rev. Lett. **108**, 080402 (2012).
[4] K. Temme, T. J. Osborne, K. G. Vollbrecht, D. Poulin, and F. Verstraete, Quantum metropolis sampling, Nature **471**, 87 (2011).
[5] M.-H. Yung and A. Aspuru-Guzik, A quantum-quantum metropolis algorithm, P. Natl. Acad. Sci. **109**, 754 (2012).
[6] M. Cerezo, A. Arrasmith, R. Babbush, S. C. Benjamin, S. Endo, K. Fujii, J. R. McClean, K. Mitarai, X. Yuan, L. Cincio, and P. J. Coles, Variational quantum algorithms, Nat. Rev. Phys. **3**, 625 (2021).
[7] J. Wu and T. H. Hsieh, Variational thermal quantum simulation via thermofield double states, Phys. Rev. Lett. **123**, 220502 (2019).
[8] G. Verdon, J. Marks, S. Nanda, S. Leichenauer, and J. Hidary, Quantum hamiltonian-based models and the variational quantum thermalizer algorithm, arXiv:1910.02071 (2019).
[9] J. R. McClean, S. Boixo, V. N. Smelyanskiy, R. Babbush, and H. Neven, Barren plateaus in quantum neural network training landscapes, Nat. Comm. **9**, 4812 (2018).
[10] A. Brabazon, M. O'Neill, and S. McGarraghy, *Natural computing algorithms*, Vol. 554 (Springer, 2015).
[11] I. M. Georgescu, S. Ashhab, and F. Nori, Quantum simulation, Rev. Mod. Phys. **86**, 153 (2014).
[12] W. Hofstetter and T. Qin, Quantum simulation of strongly correlated condensed matter systems, J. Phys. B - At. Mol. Opt. **51**, 082001 (2018).
[13] U.-J. Wiese, Ultracold quantum gases and lattice systems: quantum simulation of lattice gauge theories, Ann. Phys.-Berlin **525**, 777 (2013).
[14] B. Bauer, S. Bravyi, M. Motta, and G. K.-L. Chan, Quantum algorithms for quantum chemistry and quantum materials science, Chem. Rev. **120**, 12685 (2020).
[15] R. D. Somma, S. Boixo, H. Barnum, and E. Knill, Quantum simulations of classical annealing processes, Phys. Rev. Lett. **101**, 130504 (2008).
[16] M. H. Amin, E. Andriyash, J. Rolfe, B. Kulchytskyy, and R. Melko, Quantum boltzmann machine, Phys. Rev. X **8**, 021050 (2018).
[17] B. J. Brown, D. Loss, J. K. Pachos, C. N. Self, and J. R. Wootton, Quantum memories at finite temperature, Rev. Mod. Phys. **88**, 045005 (2016).
[18] A. Shabani and H. Neven, Artificial quantum thermal bath: Engineering temperature for a many-body quantum system, Phys. Rev. A **94**, 052301 (2016).
[19] Y. Ashida, K. Saito, and M. Ueda, Thermalization and heating dynamics in open generic many-body systems, Phys. Rev. Lett. **121**, 170402 (2018).
[20] H.-Y. Su and Y. Li, Quantum algorithm for the simulation of open-system dynamics and thermalization, Phys. Rev. A **101**, 012328 (2020).
[21] M. Metcalf, J. E. Moussa, W. A. de Jong, and M. Sarovar, Engineered thermalization and cooling of quantum many-body systems, Phys. Rev. Research **2**, 023214 (2020).
[22] L. J. Schulman, T. Mor, and Y. Weinstein, Physical limits of heat-bath algorithmic cooling, Phys. Rev. Lett. **94**, 120501 (2005).
[23] E. Kapit, Universal two-qubit interactions, measurement, and cooling for quantum simulation and computing, Phys. Rev. A **92**, 012302 (2015).
[24] A. E. Allahverdyan, R. S. Gracià, and T. M. Nieuwenhuizen, Bath-assisted cooling of spins, Phys. Rev. Lett. **93**, 260404 (2004).
[25] S. Hallgren, D. Nagaj, and S. Narayanaswami, The local hamiltonian problem on a line with eight states is qma-complete, Quantum Info. Comput. **13**, 721–750 (2013).
[26] D. Aharonov, D. Gottesman, S. Irani, and J. Kempe, The power of quantum systems on a line, Comm. Math. Phys. **287**, 41 (2009).
[27] N. Schuch, M. M. Wolf, F. Verstraete, and J. I. Cirac, Computational complexity of projected entangled pair states, Phys. Rev. Lett. **98**, 140506 (2007).
[28] S. Piddock and A. Montanaro, The complexity of antiferromagnetic interactions and 2d lattices, Quantum Info. Comput. **17**, 636–672 (2017).
[29] J. Bausch, T. Cubitt, and M. Ozols, The complexity of translationally invariant spin chains with low local dimension, Annales Henri Poincaré **18**, 3449 (2017).
[30] E. Bilgin and S. Boixo, Preparing thermal states of quantum systems by dimension reduction, Phys. Rev. Lett. **105**, 170405 (2010).
[31] A. N. Chowdhury and R. D. Somma, Quantum algorithms for gibbs sampling and hitting-time estimation, Quantum Info. Comput. **17**, 41–64 (2017).
[32] J. E. Moussa, Measurement-based quantum metropolis algorithm, arXiv:1903.01451 (2019).
[33] M. Motta, C. Sun, A. T. Tan, M. J. O'Rourke, E. Ye, A. J. Minnich, F. G. Brandão, and G. K. L. Chan, Determining eigenstates and thermal states on a quantum computer using quantum imaginary time evolution, Nature Physics **16**, 205 (2020).
[34] S.-N. Sun, M. Motta, R. N. Tazhigulov, A. T. Tan, G. K.-L. Chan, and A. J. Minnich, Quantum computation of finite-temperature static and dynamical properties of spin systems using quantum imaginary time evolution, PRX Quantum **2**, 010317 (2021).
[35] B. M. Terhal and D. P. DiVincenzo, Problem of equilibration and the computation of correlation functions on a quantum computer, Phys. Rev. A **61**, 022301 (2000).
[36] S. Polla, Y. Herasymenko, and T. E. O'Brien, Quantum digital cooling, Phys. Rev. A **104**, 012414 (2021).

[37] J. M. Deutsch, Quantum statistical mechanics in a closed system, Phys. Rev. A **43**, 2046 (1991).

[38] M. Srednicki, The approach to thermal equilibrium in quantized chaotic systems, J. Phys. A-Math. Gen. **32**, 1163 (1999).

[39] M. Srednicki, Chaos and quantum thermalization, Phys. Rev. E **50**, 888 (1994).

[40] L. D'Alessio, Y. Kafri, A. Polkovnikov, and M. Rigol, From quantum chaos and eigenstate thermalization to statistical mechanics and thermodynamics, Adv. Phys. **65**, 239 (2016).

[41] J. M. Deutsch, Eigenstate thermalization hypothesis, Rep. Prog. Phys. **81**, 082001 (2018).

[42] M. Rigol, V. Dunjko, and M. Olshanii, Thermalization and its mechanism for generic isolated quantum systems, Nature **452**, 854 (2008).

[43] T. Zhou and A. Nahum, Entanglement membrane in chaotic many-body systems, Phys. Rev. X **10**, 031066 (2020).

[44] A. Lavasani, Y. Alavirad, and M. Barkeshli, Measurement-induced topological entanglement transitions in symmetric random quantum circuits, Nat. Phys. **17**, 342 (2021).

[45] R. Movassagh, Quantum supremacy and random circuits, arXiv:1909.06210 (2019).

[46] Y. Kondo, R. Mori, and R. Movassagh, Improved robustness of quantum supremacy for random circuit sampling, arXiv:2102.01960 (2021).

[47] A. Bouland, B. Fefferman, C. Nirkhe, and U. Vazirani, On the complexity and verification of quantum random circuit sampling, Nat. Phys. **15**, 159 (2019).

[48] T. Liu, J.-G. Liu, and H. Fan, Probabilistic nonunitary gate in imaginary time evolution, Quantum Inf. Process. **20**, 1 (2021).

[49] A. M. Childs, Y. Su, M. C. Tran, N. Wiebe, and S. Zhu, Theory of trotter error with commutator scaling, Phys. Rev. X **11**, 011020 (2021).

[50] J. Zhang, J. Vala, S. Sastry, and K. B. Whaley, Exact two-qubit universal quantum circuit, Phys. Rev. Lett. **91**, 027903 (2003).

[51] R. Takagi, H. Tajima, and M. Gu, Universal sample lower bounds for quantum error mitigation, arXiv:2208.09178 (2022).

[52] While preparing this manuscript, we became aware of the recent work [53] that also studied the connections between eth and efficiency of gibbs sampling., .

[53] C.-F. Chen and F. G. Brandão, Fast thermalization from the eigenstate thermalization hypothesis, arXiv:2112.07646 (2021).

[54] V. Khemani, A. Lazarides, R. Moessner, and S. L. Sondhi, Phase structure of driven quantum systems, Phys. Rev. Lett. **116**, 250401 (2016).

[55] G. Bunin, L. D'Alessio, Y. Kafri, and A. Polkovnikov, Universal energy fluctuations in thermally isolated driven systems, Nat. Phys. **7**, 913 (2011).

[56] A. M. Childs and Y. Su, Nearly optimal lattice simulation by product formulas, Phys. Rev. Lett. **123**, 050503 (2019).

[57] E. Campbell, Random compiler for fast hamiltonian simulation, Phys. Rev. Lett. **123**, 070503 (2019).

[58] A. Skolik, J. R. McClean, M. Mohseni, P. van der Smagt, and M. Leib, Layerwise learning for quantum neural networks, Quantum Mach. Intell. **3**, 1 (2021).

[59] A. Dymarsky, Bound on eigenstate thermalization from transport, Phys. Rev. Lett. **128**, 190601 (2022).

[60] D. A. Levin and Y. Peres, *Markov chains and mixing times*, Vol. 107 (American Mathematical Soc., 2017).

[61] E. N. Economou, *Green's functions in quantum physics*, Vol. 7 (Springer Science & Business Media, 2006).

[62] K. Temme, M. J. Kastoryano, M. B. Ruskai, M. M. Wolf, and F. Verstraete, The χ_2-divergence and mixing times of quantum markov processes, J. Math. Phys. **51**, 122201 (2010).

[63] R. Arratia and L. Gordon, Tutorial on large deviations for the binomial distribution, B. Math. Biol. **51**, 125 (1989).

Supplementary Information: "Preparing thermal states on noiseless and noisy programmable quantum processors"

Oles Shtanko[1] and Ramis Movassagh[2,3]

[1] *IBM Quantum, IBM Research – Almaden, San Jose CA, 95120, USA*
[2] *IBM Quantum, MIT-IBM Watson AI lab, Cambridge MA, 02142, USA*
[3] *Google Quantum AI, Venice Beach, CA 90291, USA*

CONTENTS

I. Details of ergodic algorithm S1
A. Detailed description S1
B. Proof of Theorem S1 S3
C. Proof of Lemma S1 S6
D. Proof of Lemma S2 S6
E. Proof of Lemma S3 S7
F. Comparison to quantum Metropolis algorithm S7
G. Resource estimation S8
H. Details of simulations S8

II. Details of universal algorithm S8
A. Description and regime S8
B. Undivided Hamiltonian ($M = 1$) S9
C. Divided Hamiltonian ($M > 1$) S10
D. Success probability S12
E. Resource estimation S12
F. Details of simulation S12
G. Optimized implementation S13

III. Mapping to qubits S14

I. DETAILS OF ERGODIC ALGORITHM

In this section, we provide a detailed description of the ergodic algorithm and evaluate its performance.

A. Detailed description

The algorithm works as follows: First, the system qubits are initialized in a random state in the computational basis, while the ancilla is initialized in an easily prepared thermal state. Second, the system and the ancilla undergo d cycles of unitary evolution, with the ancilla reset to the thermal state after each cycle. Finally, the expected output of the kth cycle, $\overline{\rho}_k \equiv \mathbb{E}[\rho_k]$, satisfies the recurrence relation

$$\overline{\rho}_{k+1} = \mathcal{E}(\overline{\rho}_k) \tag{S.1}$$

expressed by the quantum channel

$$\mathcal{E}(\rho) := \mathbb{E}\,\mathrm{Tr}_a(U_k\rho\otimes\sigma_{\beta k}U_k^\dagger), \tag{S.2}$$

where U_k represents unitary evolution operators, $\sigma_{\beta k}$ is the thermal Gibbs state of the ancilla at kth cycle, Tr_a is a partial trace taken over the ancilla degrees of freedom, and the expectation is taken over random parameters of the circuit (see below for more details).

The unitary operators are given by

$$U_k = \exp(-i\mathcal{H}_k t_k), \tag{S.3}$$

where t_k represents random time intervals generated from a Poisson distribution with probability density function $p(t_k) = \gamma\exp(-\gamma t_k)$, where γ is a parameter. Additionally, $\mathcal{H}_k$ is given by Eq. (2) in the main text.

We choose the Hamiltonian for the ancilla as

$$H^k_{\mathrm{anc}} = \frac{1}{2}\sum_{m=1}^{n_a}\omega_{km}Z_m, \tag{S.4}$$

where n_a is the number of ancilla qubits, Z_m represents the Pauli-Z operator acting on the mth ancilla qubit, and $\omega_{km}\in[-\Omega,\Omega]$ are frequencies chosen independently from a uniform distribution and Ω sets the frequency

range. The thermal Gibbs state for such a Hamiltonian is a product of single-qubit states,

$$\sigma_{\beta k} = \bigotimes_{m=1}^{n_a} \Big[n(\beta\omega_{km})|0\rangle_m\langle 0|_m + n(-\beta\omega_{km})|1\rangle_m\langle 1|_m \Big], \tag{S.5}$$

where $n(x) = (1+\exp(x))^{-1}$ is a single-qubit thermal distribution. To prepare this state, one could start from the product of $|0\rangle$ states for each ancilla qubit and apply x-axis rotations to obtain the state $|\psi_k\rangle = R_k^X|0\dots 0\rangle$, where R_k^X represents the unitary operator corresponding to the x-axis rotation, applied to all ancilla qubits,

$$R_k^X(\theta) = \exp(i\theta_{k1}X_1)\otimes\cdots\otimes\exp(i\theta_{kn_a}X_{n_a}), \tag{S.6}$$

where $\theta_{km} = \arccos\sqrt{n(\beta\omega_{km})}$ and X_m is pauli-X matrix acting on the m-th ancilla qubit. After the unitary transformation, one need to implement a measurement in the computational basis and discard the result. In expectation, this step converts the pure state $|\psi_k\rangle\langle\psi_k|$ into the mixed state in Eq. (S.5).

Finally, the expectation in Eq. (S.2) is expressed as a decomposition

$$\mathbb{E} = \mathbb{E}_\omega\mathbb{E}_t\mathbb{E}_V \tag{S.7}$$

of independent averages over random times t_k ($\mathbb{E}_t$), frequencies ω_{km} ($\mathbb{E}_\omega$), and the random local operators V_{km} in Eq. (S.8) ($\mathbb{E}_V$).

In the proof of our main result, as stated in the manuscript, we assume that the matrix elements of the local coupling terms satisfy the ETH ansatz:

$$\langle\mu|V_{km}|\nu\rangle = V_\mu^{km}\delta_{\mu\nu} + \sigma_{\mu\nu}^{km}R_{\mu\nu}, \tag{S.8}$$

where $|\mu\rangle, |\nu\rangle$ are eigenstates corresponding to nearby energies $|E_\mu - E_\nu| \le \delta$ of the Hamiltonian H (the energy scale δ at which ETH applies is defined by the transport properties of the system [59]), V_μ^{km} are diagonal elements, $|\sigma_{\mu\nu}^{km}| \propto 2^{-fn}$ are the amplitudes of off-diagonal elements for some $f > 0$ that depend smoothly on the energy difference $|E_\mu - E_\nu|$, and $R_{\mu\nu} \in \mathcal{N}(0,1)$ are assumed to be independent standard gaussians. As commonly used in the literature [37, 39], the ETH assumption allows us to replace the system evolution by a self-averaging over the random matrices R, namely

$$\overline{\rho}_k \simeq \mathbb{E}_R\overline{\rho}_k. \tag{S.9}$$

We consider the regime where λ, γ, and their ratio λ^2/γ are sufficiently small. Then the steady state of the process given by Eq.(S.2) converges to the Gibbs state after averaging over the random parameters in the circuit. The convergence can be given in terms of the mixing time m to achieve the ϵ-precision of the classical Metropolis-Hastings algorithm,

$$T_{\mu\nu} = (1-\tau_\nu)\delta_{\mu\nu} + C\frac{2\pi\sigma_{\mu\nu}^2}{1+e^{\beta\Omega_{\mu\nu}}}f(\Omega_{\mu\nu}/\Omega), \tag{S.10}$$

where τ_ν are chosen such that $\sum_\mu T_{\mu\nu} = 1$, $\Omega_{\mu\nu} = E_\mu - E_\nu$ is the difference between the system's eigenenergies, and $\sigma_{\mu\nu}^2 := \mathbb{E}_V|V_{\mu\nu}|^2$. Here, $f(x)$ is Heaviside-like window function has the form

$$f(x) := \frac{1}{\pi}\Big[\arctan\Big(\frac{\Omega}{\gamma}(1-x)\Big) + \arctan\Big(\frac{\Omega}{\gamma}(1+x)\Big)\Big]. \tag{S.11}$$

For $\gamma/\Omega \ll 1$, this function is non-zero for $x \in [-1,1]$ and limits the transition between energy levels within the energy window $[-\Omega,\Omega]$. It is also an even function $f(x) = f(-x)$.

This convergence is given by Theorem 1, whose formal version writes:

Theorem S1 (formal of Theorem 1) *For any small parameter $0 < \epsilon \le 1$ for following choice of parameters*

$$\begin{aligned} d &= \tilde{O}(m^2/\epsilon),\\ \gamma^{-1} &= \tilde{O}(\beta m/\epsilon),\\ \lambda &= \tilde{O}(\epsilon^{3/2}/\beta m^{3/2}),\\ n_a &= \tilde{O}(\beta m\Omega/\epsilon), \end{aligned} \tag{S.12}$$

we have

$$\|\mathbb{E}[\rho_d] - \rho_\beta\|_1 \le \epsilon. \tag{S.13}$$

Using these scaling, the implementation physical time of the algorithm is $t = \tilde{O}(\beta m^3/\epsilon^2)$.

The proof of the theorem can be found in the following section. As part of the proof, we will show that for any state of the form $\rho = \sum_\mu p_\mu|\mu\rangle\langle\mu|$, there exists a proper choice of λ, γ, and n_a such that the process described by Eq. (S.2) satisfies

$$\mathcal{E}(\rho) \approx (1-\alpha)\sum_\mu p_\mu|\mu\rangle\langle\mu| + \alpha\sum_{\mu\nu}T_{\mu\nu}p_\nu|\mu\rangle\langle\mu|, \tag{S.14}$$

where the transition amplitudes $T_{\mu\nu}$ correspond to a classical Metropolis-Hastings algorithm in Eq. (S.10) and

$$\alpha = \frac{n_a\lambda^2}{\gamma\Omega C} \ll 1 \tag{S.15}$$

is a small parameter. Note that C is a constant with an arbitrary positive value, since it does not affect the map in Eq. (S.14). However, it is crucial to choose C such that $\tau_\nu \ge 0$ ensures that $T_{\mu\nu}$ can be interpreted as the transition matrix for a stochastic process.

Using Eq. (S.14), we will show that for sufficiently large values of d, the expected output of the circuit is well approximated by $\overline{\rho}_d \simeq \sum_\mu p_\mu^{(r)}|\mu\rangle\langle\mu|$, where the probabilities $p_\mu^{(r)}$ are generated by $r \propto \alpha d$ Metropolis update steps defined by the matrix T in Eq. (S.10). Any transition matrix T with strictly positive entries is known to be a contractive map [60] characterized by a non-zero gap Δ. For any such map, the mixing time is $m \propto 1/\Delta$ with a

prefactor that scales at most linearly with the number of qubits. Since under ETH $\sigma^2_{\mu\nu}$ are positive functions of the energy difference $\Omega_{\mu\nu}$, one can deduce from Eq. (S.10) that $T_{\mu\nu} > 0$. The contractive property together with the classical detailed balance condition imply that Eq. (S.14) leads to a unique steady state that is ϵ-close to the Gibbs state.

We evaluate the gap for T in Eq. (S.10) for a size-limited numerical simulation of the hardcode Bose-Hubbard Hamiltonian in Eq. (7) as shown in Fig. 1 of the main text. We focus only on the reduced space including $n/2$ bosons and as V_{km} we use the density operators $n_i = a_i^\dagger a_i$ and obtain

$$T_{\mu\nu} = (1-\tau_\nu)\delta_{\mu\nu} + C\frac{f(\Omega_{\mu\nu}/\Omega)}{1+e^{\beta\Omega_{\mu\nu}}}\frac{1}{n}\sum_{i=1}^{n}|\langle\mu|n_i|\nu\rangle|^2, \quad \text{(S.16)}$$

where we have chosen C so that $\max(\sum_\mu \tau_{\mu\nu}) = 1$. This simulation suggests that the gap has a reasonable polynomial scaling with system size.

B. Proof of Theorem S1

As a first step, it is convenient to represent the unitary transformation in Eq. (S.3) using the Liouville superoperator $\mathcal{L}_k(\rho) = -i[\mathcal{H}_k, \rho]$. Then we can rewrite

$$U_k \rho U_k^\dagger = \exp(\mathcal{L}_k t_k)(\rho). \quad \text{(S.17)}$$

Next, we use the decomposition $\mathcal{L}_k = \mathcal{L}_k^0 + \lambda\mathcal{L}_k^1$, following the structure of the Hamiltonian in Eq. (2) in the main text. Here,

$$\begin{aligned}\mathcal{L}_k^0(\rho) &= -i\Big[H\otimes I_{\text{anc}} + I_{\text{sys}}\otimes H^k_{\text{anc}},\ \rho\ \Big],\\ \mathcal{L}_k^1(\rho) &= -i\sum_{m=1}^{n_a}[V_{km}\otimes X_m, \rho],\end{aligned} \quad \text{(S.18)}$$

and I_{sys}, I_{anc} are the identity operators on the spaces of system and ancilla qubits, respectively.

The main channel (Eq.(S.2)) in the superoperator representation includes expectation given by Eq. (S.7) and can be written as

$$\begin{aligned}\mathcal{E}(\rho) &= \mathbb{E}_V\mathbb{E}_\omega\mathbb{E}_t \text{Tr}_a\left[\exp(\mathcal{L}_k t)\,(\rho\otimes\sigma_{\beta k})\right]\\ &= \gamma\mathbb{E}_V\mathbb{E}_\omega\int_0^\infty dt e^{-\gamma t}\text{Tr}_a\left[\exp(\mathcal{L}_k t)\,(\rho\otimes\sigma_{\beta k})\right]\\ &= \gamma\mathbb{E}_V\mathbb{E}_\omega\text{Tr}_a\left[\frac{1}{\gamma-\mathcal{L}_k^0-\lambda\mathcal{L}_k^1}\,(\rho\otimes\sigma_{\beta k})\right],\end{aligned} \quad \text{(S.19)}$$

where we used the Laplace transform of the exponential function to express the cycle time average.

The next step is to express the propagator in Eq. (S.19) as a Dyson's series in terms of the parameter λ [61], resulting in

$$\frac{1}{\gamma-\mathcal{L}_k^0-\lambda\mathcal{L}_k^1} = \frac{1}{\gamma-\mathcal{L}_k^0}\sum_{\ell=0}^{\infty}\lambda^\ell\Big(\mathcal{L}_k^1\frac{1}{\gamma-\mathcal{L}_k^0}\Big)^\ell. \quad \text{(S.20)}$$

When we insert this series into Eq. (S.19), we observe that all contributions from odd $\ell \in 2\mathbb{N}+1$ vanish exactly. This result stems from the fact that the ancilla is initialized in the computational basis and the superoperator $\mathcal{L}_k^1$ is proportional to the Pauli-X operator acting on either the left or right side of the density operator of a single ancilla qubit. As a result, odd numbers of $\mathcal{L}_k^1$ always produce a matrix with zero diagonals, which then vanish upon partial trace.

Then, the expression in Eq. (S.19) can be written as

$$\mathcal{E}(\rho) = C_0(\rho) + \lambda^2 C_2(\rho) + \lambda^4 C_4(\rho), \quad \text{(S.21)}$$

where $C_0(\cdot)$, $C_2(\cdot)$, and $C_4(\cdot)$ are linear maps defined as

$$\begin{aligned}C_0(\rho) &:= \gamma\frac{1}{\gamma-\mathcal{L}_k^0}(\rho),\\ C_2(\rho) &:= \gamma\,\mathbb{E}_V\mathbb{E}_\omega\text{Tr}_a\left[\Big(\frac{1}{\gamma-\mathcal{L}_k^0}\mathcal{L}_k^1\Big)^2\frac{1}{\gamma-\mathcal{L}_k^0}\,(\rho\otimes\sigma_{\beta k})\right],\end{aligned} \quad \text{(S.22)}$$

and

$$C_4(\rho) := \gamma\mathbb{E}_V\mathbb{E}_\omega\text{Tr}_a\left[\Big(\frac{1}{\gamma-\mathcal{L}_k^0}\mathcal{L}_k^1\Big)^4\frac{1}{\gamma-\mathcal{L}_k}\,(\rho\otimes\sigma_{\beta k})\right]. \quad \text{(S.23)}$$

In the last expression, the rightmost propagator contains the full Liouvillian operator $\mathcal{L}_k$, accounting for the higher orders in the perturbation series, making the equality in Eq. (S.21) exact.

We now analyze the action of the perturbation $\mathcal{L}_k^1$ and the unperturbed propagator $\mathcal{L}_k^0$ on a basis state. First, the action of the perturbation is

$$\begin{aligned}&\mathcal{L}_k^1\Big(|\mu\rangle\langle\nu|\otimes|\mathbf{a}\rangle\langle\mathbf{b}|\Big)\\ &\quad= -i\sum_{\delta,m}V^{km}_{\delta\mu}|\delta\rangle\langle\nu|\otimes|..1-a_m..\rangle\langle..b_m..|\\ &\qquad+ i\sum_{\delta,m}V^{km}_{\nu\delta}|\mu\rangle\langle\delta|\otimes|..a_m..\rangle\langle..1-b_m..|,\end{aligned} \quad \text{(S.24)}$$

where $|\mu\rangle$ are the eigenstates of the target Hamiltonian H and $|\mathbf{a}\rangle = |a_1\dots a_{n_a}\rangle$ are the eigenstates of the ancilla Hamiltonian, which are product states in the computational basis. We also used the notation $V^{km}_{\mu\nu} := \langle\mu|V_{km}|\nu\rangle$. Also, we use the expression

$$\frac{1}{\gamma-\mathcal{L}_k^0}|\mu\rangle\langle\nu|\otimes|\mathbf{a}\rangle\langle\mathbf{b}| = \frac{1}{\gamma+i(\Omega_{\mu\nu}+\omega_{\mathbf{ab}})}|\mu\rangle\langle\nu|\otimes|\mathbf{a}\rangle\langle\mathbf{b}|, \quad \text{(S.25)}$$

where $\Omega_{\mu\nu} = E_\mu - E_\nu$, $\omega_{\mathbf{ab}} = e_{\mathbf{a}} - e_{\mathbf{b}}$, and $e_{\mathbf{a}}$ are the eigenenergies of the ancilla Hamiltonian.

The action of the second maps is

$$C_2(|\nu\rangle\langle\nu'|) := \gamma\mathbb{E}_\omega\mathbb{E}_V \sum_{m=1}^{n_a}\sum_{s=\pm1}\frac{n(s\omega_{km})}{\gamma+i\Omega_{\nu\nu'}}\times \sum_{\alpha\mu}\Bigg(\frac{V^{km}_{\mu\nu}V^{km}_{\nu'\alpha}|\mu\rangle\langle\alpha|}{(\gamma+i(\Omega_{\mu\nu'}-s\omega_{km}))(\gamma+i\Omega_{\mu\alpha})} + \frac{V^{km}_{\nu'\mu}V^{km}_{\alpha\nu}|\alpha\rangle\langle\mu|}{(\gamma+i(\Omega_{\nu\mu}+s\omega_{km}))(\gamma+i\Omega_{\alpha\mu})} - \frac{V^{km}_{\mu\nu}V^{km}_{\alpha\mu}|\alpha\rangle\langle\nu'|}{(\gamma+i(\Omega_{\mu\nu'}-s\omega_{km}))(\gamma+i\Omega_{\alpha\nu'})} - \frac{V^{km}_{\nu'\mu}V^{km}_{\mu\alpha}|\nu\rangle\langle\alpha|}{(\gamma+i(\Omega_{\nu\mu}+s\omega_{km}))(\gamma+i\Omega_{\nu\alpha})}\Bigg). \tag{S.26}$$

Next, we use the ETH assumption to ensure that

$$C_2(\rho) \simeq \mathbb{E}_R C_2(\rho). \tag{S.27}$$

In particular, this assumption implies that

$$\mathbb{E}_R V^{km}_{\mu\nu}V^{km}_{\nu'\mu'} = (V^{km}_\mu)^2\delta_{\mu\nu}\delta_{\mu'\nu'} + (\sigma^{km}_{\mu\nu})^2\delta_{\mu\mu'}\delta_{\nu\nu'}. \tag{S.28}$$

Let us consider the contributions for the diagonal and off-diagonal entries only,

$$C_2(|\nu\rangle\langle\nu|) = 2\mathbb{E}_\omega\sum_\mu\sum_{s=\pm1}\sum_{m=1}^{n_a}\sigma^2_{\mu\nu}\times \frac{n(s\omega_{km})}{(s\omega_{km}-\Omega_{\mu\nu})^2+\gamma^2}\Big(|\mu\rangle\langle\mu| - |\nu\rangle\langle\nu|\Big), \tag{S.29}$$

where we defined

$$\sigma^2_{\mu\nu} := \mathbb{E}_V\Big\{(\sigma^{km}_{\mu\nu})^2 + (V^{km}_\mu)^2\delta_{\mu\nu}\Big\} \simeq \mathbb{E}_V|V_{\mu\nu}|^2. \tag{S.30}$$

Note that this transformation does not depend on the diagonal terms. The next step would be to calculate the expectation $\mathbb{E}_\omega$ over the frequencies of the ancilla qubits, which can be done with the formula

$$\mathbb{E}_\omega := \frac{1}{(2\Omega)^{n_a}}\int_{-\Omega}^{\Omega}d\omega_{k1}\cdots\int_{-\Omega}^{\Omega}d\omega_{kn_a}. \tag{S.31}$$

The corresponding integrals can subsequently be computed by employing the subsequent result:

Lemma S1 *Assume $\beta\gamma \ll 1$. Then*

$$\int_{-\Omega}^{\Omega}\frac{d\omega n(\beta\omega)}{(\omega-\Omega_{\mu\nu})^2+\gamma^2} = \frac{\pi}{\gamma}\Big(n(\beta\Omega_{\mu\nu})f(\Omega_{\mu\nu}/\Omega) + O(\beta\gamma)\Big), \tag{S.32}$$

where $f(x)$ is defined in Eq. (S.11)*.*

In Section I C, we provide a proof of this Lemma. With the help of its results, we can transform Eq. (S.29) into

$$\lambda^2 C_2\big(|\nu\rangle\langle\nu|\big) = \frac{2\pi n_a\lambda^2}{\Omega\gamma}\sum_\mu\sigma^2_{\mu\nu}n(\Omega_{\mu\nu})f(\Omega_{\mu\nu}/\Omega) \times\Big(|\mu\rangle\langle\mu| - |\nu\rangle\langle\nu|\Big) + O\Big(\frac{\beta\lambda^2 n_a}{\Omega}\Big). \tag{S.33}$$

where, here and below, we use O-notation for quantum states and operators in a sense of the *trace norm* of the remaining terms.

As we will see below, the last O-small term constitute a part of algorithm's error. Next, we choose main parameters to be functions of ϵ' with scaling

$$n_a = O(\beta\Omega/\epsilon'), \quad \gamma^{-1} = O(\beta/\epsilon'), \quad \lambda = O(\epsilon'^{3/2}/\beta). \tag{S.34}$$

This choice allows us to rewrite the scaling of the error terms in Eq. (S.33) as

$$\frac{\lambda^2 n_a}{\gamma\Omega} = O(\epsilon'), \qquad \frac{\beta\lambda^2 n_a}{\Omega} = O(\epsilon'^2) \tag{S.35}$$

Let us assume now that the expected density matrix $\overline{\rho}_k$ is nearly diagonal in the energy basis, i.e.

$$\overline{\rho}_k = \tilde{\rho}_k + \delta\rho_k, \qquad \tilde{\rho}_k = \sum_\mu p_{k\mu}|\mu\rangle\langle\mu|. \tag{S.36}$$

where $p_{k\mu}$ are non-negative occupations of the energy levels and $\delta\rho_k$ are small corrections that satisfy $\|\delta\rho_k\|_1 \le \epsilon_k$. From Eqs. (S.33) and (S.35), it follows that the diagonal part undergoes transformation as

$$\lambda^2 C_2(\tilde{\rho}_k) = \alpha\sum_{\mu\nu}\tau_{\mu\nu}p_{k\nu}\Big(|\mu\rangle\langle\mu| - |\nu\rangle\langle\nu|\Big) + O(\epsilon'^2). \tag{S.37}$$

where we used the definition of α in Eq. (S.15) and amplitudes $\tau_{\mu\nu}$ in Eq. (S.10). Note that $\alpha = O(\epsilon')$, the property that we will use later.

At the same time, the effect of C_2 on the non-diagonal correction can be characterized by the following Lemma.

Lemma S2 *Given the scaling of the parameters γ^{-1}, λ, and n_a in Eq.* (S.35)*, for any $\delta\rho$, it follows that*

$$\lambda^2\|C_2(\delta\rho)\|_1 = \tilde{O}\left(\epsilon'\|\delta\rho\|_1\right). \tag{S.38}$$

The proof of this Lemma can be found in Section. I D below. Combining these two expressions, we get

$$\lambda^2 C_2(\overline{\rho}_k) = \alpha\sum_{\mu\nu}\tau_{\mu\nu}p_{k\nu}\Big(|\mu\rangle\langle\mu| - |\nu\rangle\langle\nu|\Big) + \tilde{O}(\epsilon'\epsilon_k) + \tilde{O}(\epsilon'^2). \tag{S.39}$$

Next, we utilize the following Lemma to establish the bound for the operator $C_4(\rho)$.

Lemma S3 *Given the scaling of the parameters in Eq.* (S.35)*, for any density operator ρ, it follows that*

$$\lambda^4 \|C_4(\rho)\|_1 = \tilde{O}(\epsilon'^2). \tag{S.40}$$

The proof can be found in Sec. E below. Using the recurrence relation in Eq. (S.1), we derive that

$$\overline{\rho}_{k+1} = \tilde{\rho}_k + C_0(\delta\rho_k) + \alpha \sum_{\mu\nu} \tau_{\mu\nu} p_{k\nu} \Big(|\mu\rangle\langle\mu| - |\nu\rangle\langle\nu| \Big) + \tilde{O}(\alpha\epsilon_k) + \tilde{O}(\epsilon'^2), \tag{S.41}$$

In terms of the diagonal part and the magnitude of the correction in Eq. (S.36), this relation van be written in the form

$$\begin{aligned} \tilde{\rho}_{k+1} &= \mathcal{V}(\tilde{\rho}_k), \\ \epsilon_{k+1} &= \epsilon_k + O(\epsilon'\epsilon_k) + \tilde{O}(\epsilon'^2), \end{aligned} \tag{S.42}$$

where $\mathcal{V} = (1-\alpha)\mathcal{I} + \alpha\mathcal{T}$, and action of the map $\mathcal{T}$ on the diagonal matrix is defined as

$$\mathcal{T}(\tilde{\rho}_k) = \sum_{\nu} T_{\mu\nu} p_{k\nu} |\mu\rangle\langle\mu|, \tag{S.43}$$

where $T_{\mu\nu}$ is defined in Eq. (S.10). By iterating this map while assuming $\epsilon_0 = 0$, we arrive at

$$\overline{\rho}_k = \mathcal{V}^k(\rho_0) + \delta\rho_k, \qquad \|\delta\rho_k\|_1 = \tilde{O}(k\epsilon'^2). \tag{S.44}$$

The first term is represented by the map

$$\mathcal{V}^k = \Big((1-\alpha)\mathcal{I} + \alpha\mathcal{T}\Big)^k = \sum_{l=0}^{k} p(l;k,\alpha)\mathcal{T}^l, \tag{S.45}$$

where $\mathcal{I}$ represents the identity superoperator and $p(l;k,\alpha)$ are probabilities from the binomial distribution,

$$p(l;k,\alpha) := \binom{k}{l} \alpha^l (1-\alpha)^{k-l}. \tag{S.46}$$

By using the triangle inequality, we bound the difference between the main part of the Gibbs state ρ_β as

$$\begin{aligned} \|\mathcal{V}^k(\rho_0) - \rho_\beta\|_1 &\le \Big\| \sum_{l=0}^{k} p(l;k,\alpha)(\mathcal{T}^l(\rho_0) - \rho_\beta) \Big\|_1 \\ &\le \sum_{l=0}^{k} p(l;k,\alpha) \Big\| \mathcal{T}^l(\rho_0) - \rho_\beta \Big\|_1 \end{aligned} \tag{S.47}$$

Next, we use the inequality [62]

$$\Big\| \mathcal{T}^l(\rho_0) - \rho_\beta \Big\|_1 \le q_n (1-\Delta)^\ell \tag{S.48}$$

where Δ is the gap of the process $\mathcal{T}$ and q_n is a constant that grows exponentially with the number of qubits n. This leads us to

$$\|\mathcal{V}^k(\rho_0) - \rho_\beta\|_1 \le q_n \sum_{l=0}^{k} p(l;k,\alpha)(1-\Delta)^\ell. \tag{S.49}$$

By choosing certain integer $0 < s < k$, we divide the sum into two parts as

$$\|\mathcal{V}^k(\rho_0) - \rho_\beta\|_1 \le q_n \sum_{l=0}^{s} p(l;k,\alpha)(1-\Delta)^\ell + q_n \sum_{l=s+1}^{k} p(l;k,\alpha)(1-\Delta)^\ell. \tag{S.50}$$

Each sum can be bounded by taking the smallest value in the exponent of $(1-\Delta)$, resulting in

$$\|\mathcal{V}^k(\rho_0) - \rho_\beta\|_1 \le q_n \Big(\sum_{l=0}^{s} p(l;k,\alpha) + (1-\Delta)^\ell \Big). \tag{S.51}$$

For all $s \le \alpha k$, we can utilize the Chernoff bound for the binomial distribution [63] in the form

$$\sum_{l=0}^{s} p(l;k,\alpha) \le \exp\Big(-kD\left(\frac{s}{k} \| \alpha\right) \Big), \tag{S.52}$$

where $D(p\|p')$ represents the Kullback-Leibler divergence between two biased binary distributions, characterized by probabilities p and p', i.e.

$$D(p\|p') = p \log \frac{p}{p'} + (1-p) \log \frac{1-p}{1-p'}. \tag{S.53}$$

Now, let us choose the division parameter to be $s = \mu\alpha k$, where $0 < \mu \le 1$ is a constant. Then

$$D\left(\frac{s}{k}\|\alpha\right) = D(\mu\alpha\|\alpha) \ge f(\mu)\alpha, \tag{S.54}$$

where $f(\mu) := 1 - \mu + \mu\log\mu$ is a non-negative function for $\mu \in (0,1]$. By utilizing this property, we can state that

$$\sum_{l=0}^{\mu\alpha k} p(l;k,\alpha) \le \exp\left(-f(\mu)\alpha k\right), \tag{S.55}$$

and therefore, the distance in Eq. (S.47) satisfies

$$\|\mathcal{V}^k(\rho_0) - \rho_\beta\|_1 \le q_n e^{-O(\alpha k \Delta)}. \tag{S.56}$$

We will now recall the definition of α from Eq. (S.15) and use the scaling in Eq. (S.35) to show that $\alpha = O(\epsilon')$. This implies that the distance between the output of the algorithm at step d and the Gibbs state is bounded by

$$\|\rho_d - \rho_\beta\|_1 \le q_n e^{-O(\Delta\epsilon' d)} + \tilde{O}(d\epsilon'^2) := \epsilon, \tag{S.57}$$

where ϵ is our target error. To compensate for the exponentially large q_n factor, we need certain $d = O(m\epsilon')$, where $m = \tilde{O}(\log q_n/\Delta)$ is mixing time. Another consition is that the contribution from the second term is small, $\epsilon = \tilde{O}(\epsilon'^2 d)$. These conditions can be satisfied together if

$$d = \tilde{O}(m^2/\epsilon), \qquad \epsilon' = \tilde{O}(\epsilon/m). \tag{S.58}$$

Substituting this error measure into Eq. (S.34), we obtain the required scaling of the parameters

$$\gamma^{-1} = \tilde{O}(\beta m/\epsilon), \quad \lambda = \tilde{O}(\epsilon^{3/2}/\beta m^{3/2}), \tag{S.59}$$

Finally, the average time of the algorithm must be scaled as $t := d/\gamma = O(\beta m^3/\epsilon^2)$. This completes our proof.

C. Proof of Lemma S1

We first rewrite the integral as

$$\begin{aligned}\int_{-\Omega}^{\Omega} d\omega \frac{n(\beta\omega)}{(\omega-\Omega_{\mu\nu})^2+\gamma^2} &= \int_{-\Omega}^{\Omega} d\omega \frac{n(\beta\Omega_{\mu\nu})}{(\omega-\Omega_{\mu\nu})^2+\gamma^2} \\ &+ \int_{-\Omega}^{\Omega} d\omega \frac{n(\beta\omega)-n(\beta\Omega_{\mu\nu})}{(\omega-\Omega_{\mu\nu})^2+\gamma^2} \\ &= \frac{\pi}{\gamma}\Big(n(\Omega_{\mu\nu}) f(\Omega_{\mu\nu}/\Omega) + \beta\gamma F(\beta\Omega_{\mu\nu}, \beta\gamma, \beta\Omega)\Big),\end{aligned} \tag{S.60}$$

we have used the notation

$$F(z_0, g, W) := \int_{-W}^{W} dz \frac{n(z+z_0)-n(z_0)}{z^2+g^2}. \tag{S.61}$$

It is straightforward to show that

$$\int_{-\Omega}^{\Omega} d\omega \frac{1}{(\omega-\Omega_{\mu\nu})^2+\gamma^2} = \frac{\pi}{\gamma} f(\Omega/\Omega_{\mu\nu}), \tag{S.62}$$

where $f(x)$ is defined in Eq. (S.11).

Our next objective is to demonstrate that the integral in Eq. (S.61) is bounded by a constant independent of z_0, W, or g. Since the denominator is symmetric with respect to zero, we can rewrite the integral as

$$F(z_0, g, W) = \int_{-W}^{W} \frac{f(z, z_0)}{z^2+g^2} dz, \tag{S.63}$$

where we have denoted the symmetrized numerator as

$$\begin{aligned} f(z, z_0) :&= \frac{1}{2}\Big(n(z+z_0) + n(-z+z_0) - 2n(z_0)\Big) \\ &= \frac{1}{2} \frac{\tanh(z_0/2)(\cosh z - 1)}{2\cosh^2(z_0/2) + \cosh z - 1}.\end{aligned} \tag{S.64}$$

The absolute value of the integral obeys the bound

$$|F(z_0, g, W)| \leq \frac{1}{2} |\tanh(z_0/2)| \int_{\infty}^{-\infty} \frac{z^2 dz}{(z^2+g^2)(z^2+A^2(z))}, \tag{S.65}$$

where $A^2(z) = 2z^2\cosh^2(z_0/2)/(\cosh z - 1)$ and we extended the limits of integration as the integrand is non-negative. Utilizing the facts that $z^2+g^2 \geq z^2$ and $|\tanh(z_0/2)| \leq 1$, we obtain

$$|F(z_0, g, W)| \leq \frac{1}{2}\int_{-\infty}^{\infty} \frac{dz}{z^2+A^2(z)}. \tag{S.66}$$

Since $A(z)$ monotonically decreases with z, for any $z' > 0$, we can rewrite

$$\begin{aligned}|F(z_0, g, W)| &\leq \int_{-\infty}^{z'} \frac{dz}{z^2+A^2(z)} + \int_{z'}^{\infty} \frac{dz}{z^2+A^2(z)} \\ &< \int_{-\infty}^{z'} \frac{dz}{z^2+A^2(z')} + \int_{z'}^{\infty} \frac{dz}{z^2} \\ &= \frac{\arctan(z'/A(z'))}{A(z')} + \frac{1}{z'}.\end{aligned} \tag{S.67}$$

Since $\arctan(x) \leq \pi/2$ for all x and $A(z') \geq \sqrt{2z'^2/(\cosh z' - 1)}$, we write

$$|F(z_0, g, W)| < \frac{\pi}{2}\sqrt{\frac{\cosh z' - 1}{2z'^2}} + \frac{1}{z'}. \tag{S.68}$$

For any $0 < z' < \infty$, the right-hand side is a constant that attains its minimum value of approximately 1.4045. This bound, however, is not particularly tight, as a quick numerical check suggests that $|F(z_0, g)| \lesssim 0.441$. Nevertheless, this result enables us to establish that

$$\int_{-\Omega}^{\Omega} \frac{d\omega n(\beta\omega)}{(\omega-\Omega_{\mu\nu})^2+\gamma^2} = \frac{\pi}{\gamma}\Big(n(\Omega_{\mu\nu}) f(\Omega_{\mu\nu}/\Omega) + O(\beta\gamma)\Big). \tag{S.69}$$

This concludes the proof.

D. Proof of Lemma S2

We can rewrite the trace norm using the definition given in Eq. (S.22) as

$$\|C_2(\delta\rho)\|_1 = \gamma \|\mathbb{E}_\omega \mathbb{E}_V \mathrm{Tr}_a (\mathcal{G}_k^0 \mathcal{L}_k^1)^2 \mathcal{G}_k^0 (\delta\rho \otimes \sigma_{\beta k})\|_1 \tag{S.70}$$

Using the superoperator structure, we get

$$\begin{aligned}\|C_2(\delta\rho)\|_1 \leq \gamma \sum_m \sum_{s,s'=\pm 1} \mathbb{E}_\omega \mathbb{E}_V \|\tilde{\mathcal{G}}_0^k(0) \mathcal{V}_{km}^s \tilde{\mathcal{G}}_0^k(s\omega_{km}) \\ \mathcal{V}_{km}^{s'} \tilde{\mathcal{G}}_0^k(0) \delta\rho\|_1\end{aligned} \tag{S.71}$$

where we used the following notation for the "displaced" Green's function,

$$\tilde{\mathcal{G}}_0^k(\omega) := \frac{1}{\gamma - \mathcal{L}_k^0 - i\omega}, \tag{S.72}$$

and the notation of the left and right actions of the coupling operator,

$$\mathcal{V}_{km}^+ := V_{km} \otimes I, \qquad \mathcal{V}_{km}^- := I \otimes V_{km}. \tag{S.73}$$

Next, we can upper bound the action of the operator C_2 on the hermitian operator $\delta\rho$ as

$$\|C_2(\delta\rho)\|_1 \leq 4\gamma \sum_m \sum_{s=\pm 1} \mathbb{E}_V \sigma^2_{\max}[\tilde{\mathcal{G}}^k_0(0)]\sigma_{\max}[\mathbb{E}_\omega \tilde{\mathcal{G}}^k_0(s\omega_{km})] \times \|V_{km}\|^2 \|\delta\rho\|_1 \tag{S.74}$$

where $\sigma_{\max}(\mathcal{A})$ denotes the largest singular eigenvalue of the superoperator $\mathcal{A}$. Using the explicit form of the suoperoperator in Eq. (S.72), we can derive that

$$\begin{aligned} &\sigma_{\max}[\tilde{\mathcal{G}}^k_0(0)] \leq \frac{1}{\gamma}, \\ &\sigma_{\max}[\mathbb{E}_\omega \tilde{\mathcal{G}}^k_0(\omega)] = \frac{1}{2\Omega}\max_{\mu,\nu}\left|\int_{-\Omega}^{\Omega} \frac{d\omega}{\gamma - i(\Omega_{\mu\nu}+\omega)}\right| \\ &\qquad = O\left(\frac{1}{\Omega}\log\frac{\Omega}{\gamma}\right). \end{aligned} \tag{S.75}$$

Using this scaling, we arrive at the expression

$$\|C_2(\delta\rho)\|_1 = O\left(\frac{\lambda^2 n_a}{\gamma\Omega}\log\frac{\Omega}{\gamma}\|\delta\rho\|_1\right) = \tilde{O}(\epsilon'\|\delta\rho\|_1). \tag{S.76}$$

To make the last step, we used the proper scaling of the parameters from Eq. (S.35). This expression conlcudes our proof.

E. Proof of Lemma S3

Using this density matrix, we can rewrite the action of the channel as $C_4(\rho) = \sum_{b=1}^{\infty} C_4^{(b)}(\rho)$, where

$$C_4^{(b)}(\rho) = \gamma \mathbb{E}_V \mathbb{E}_\omega \mathrm{Tr}_a\left[\left(\mathcal{G}^k_0 \mathcal{L}^1_k\right)^{2+2b} \mathcal{G}^0_k(\rho\otimes\sigma_{\beta k})\right]. \tag{S.77}$$

where $\mathcal{G}^0_k := 1/(\gamma - \mathcal{L}^0_k)$.

Next we decompose the coupling superoperator as a sum over individual couplings to each ancilla qubit, i.e.

$$\mathcal{L}^1_k = \sum_{m=1}^{n_a} \mathcal{L}^1_{mk}, \tag{S.78}$$

which allows us to rewrite the channel using two components

$$\lambda^4 C_4^{(1)}(\rho) = S_1(\rho) + S_2(\rho). \tag{S.79}$$

Each component corresponds to a different number of distinct operators $\mathcal{L}^1_{km}$. For example, the first term has the form

$$S_1(\rho) = \gamma \mathbb{E}_V \frac{\lambda^4}{2\Omega}\sum_{m=1}^{n_a}\int_{-\Omega}^{\Omega} d\omega_{km} \mathrm{Tr}_a\left[\left(\mathcal{G}^k_0\mathcal{L}^1_{km}\right)^4 \mathcal{G}^0_k(\rho\otimes\sigma_{\beta k})\right]. \tag{S.80}$$

The expression on the right has one integral over frequencies ω_{km} and four poles in the form $1/(\omega_{km} \pm i\gamma + \dots)$ for each operator $\mathcal{G}^0_k$. Taking the integral eliminates one of the poles leading to the expression in Eq. (S.75), while the remaining poles generate at most $O(\gamma^{-3})$ divergence in the limit $\gamma \to \infty$. As a result, this term behaves as

$$\|S_1(\rho)\|_1 = O\left(\frac{\lambda^4 n_a}{\gamma^3\Omega}\log\frac{\Omega}{\gamma}\right) = \tilde{O}(\epsilon'^2), \tag{S.81}$$

where the factor of n_a is due to the sum taken over ancilla qubits.

Next, the second term involves operators $\mathcal{L}^1_{km}$ for two distinct values of m, and can be written as

$$\begin{aligned} S_2(\rho) = \gamma\mathbb{E}_V \frac{\lambda^4}{4\Omega^2}\tilde{\sum_{m_1,m_2}}\int_{-\Omega}^{\Omega} d\omega_{km_1}\int_{-\Omega}^{\Omega} d\omega_{km_2}\times \\ \Bigg(\mathrm{Tr}_a\left[\left(\mathcal{G}^0_k\mathcal{L}^1_{km_1}\right)^2\left(\mathcal{G}^0_k\mathcal{L}^1_{km_2}\right)^2\mathcal{G}^0_k(\rho\otimes\sigma_{\beta k})\right] \\ + \mathrm{Tr}_a\left[\left(\mathcal{G}^0_k\mathcal{L}^1_{km_1}\mathcal{G}^0_k\mathcal{L}^1_{km_2}\right)^2\mathcal{G}^0_k(\rho\otimes\sigma_{\beta k})\right]\Bigg), \end{aligned} \tag{S.82}$$

where here and below the sum $\tilde{\sum}_{m_1\dots m_2}$ is taken over all values of m_i such that $m_1 \neq m_2$. Using the same analysis, we conclude that this expression has two pole-reducing integrals and four poles in total, and therefore has a divergence of $O(\gamma^{-2})$. The resulting bound is

$$\|S_2(\rho)\|_1 = O\Big(\frac{n_a^2\lambda^4}{\gamma^2\Omega^2}\log^2\frac{\Omega}{\gamma}\Big) = \tilde{O}(\epsilon'^2). \tag{S.83}$$

Application of the triangle inequality gives

$$\lambda^4\|C_4^{(1)}(\rho)\|_1 \leq \|S_1(\rho)\|_1 + \|S_2(\rho)\|_1 = \tilde{O}(\epsilon'^2). \tag{S.84}$$

In a similar fashion, the contributions of higher-order terms are

$$\|C_4^{(b)}\|_1 = \tilde{O}\left(\frac{\lambda^{2+2b}}{\gamma^{2+2b}}\mathrm{poly}\Big(\frac{n_a\gamma}{\Omega}\log\frac{\Omega}{\gamma}\Big)\right) = \tilde{O}(\epsilon'^{1+b}). \tag{S.85}$$

Assuming that the Dyson's series converges, we get

$$C_4(\rho) = \tilde{O}(\epsilon'^2). \tag{S.86}$$

This expression concludes the proof.

F. Comparison to quantum Metropolis algorithm

In this section, we compare the performance of our algorithm to that of the quantum Metropolis algorithm presented in Ref. [4]. Quantum Metropolis algorithms iteratively implement a quantum map $\mathcal{E}_{QM}$ that satisfies conditions similar to the detailed balance conditions of its classical counterpart. The authors provide an estimate of the distance between the fixed point σ^* of the map $\mathcal{E}_{QM}$, i.e. $\mathcal{E}_{QM}(\sigma^*) = \sigma^*$, and the Gibbs state as

$$\epsilon := \|\sigma^* - \rho_\beta\| \leq \frac{\epsilon_{sg}}{1-\eta}, \tag{S.87}$$

where η is contraction parameter of the single-step quantum Metropolis map (i.e. for all ρ, σ it satisfies $\|\mathcal{E}_{QM}(\rho-\sigma)\|_1 \leq \eta\|\rho-\sigma\|_1$) and ϵ_{sg} is the error of a single quantum Metropolis step. This error has the following scaling

$$\epsilon_{sg} = O\big(\beta m_{QM}/T\big), \tag{S.88}$$

where m_{QM} is the mixing time of the quantum Metropolis process and T is the time of implementation of a single step. The total time of the quantum Metropolis algorithm scales as

$$t_{QM} \propto mT = O\Big(\frac{\beta m_{QM}^2}{(1-\eta)\epsilon}\Big). \tag{S.89}$$

We can compare this time to the runtime of our algorithm, $t = O(\beta m^3/\epsilon^2)$. Our algorithm has a more restrictive scaling with the target error compared to the quantum Metropolis algorithm, which has only a linear scaling. It is worth noting that the $1/\epsilon$ error in Eq. (S.87) ignores the mixing error that we take into account. It is also difficult to compare the scaling of $m_{QM}^2/(1-\eta)$ for the quantum Metropolis algorithm with the scaling factor m^3 in our problem. However, it is easier to find m by analyzing the classical stochastic process represented by the transition matrix T in our case. Both algorithms are likely to have polynomial factors for a wide range of quantum Hamiltonians.

G. Resource estimation

Let us summarize the resources needed to implement the algorithm. As in the main text, n is the number of qubits for the target Hamiltonian, β is the inverse temperature, and ϵ is the error of the algorithm.

Type of Hamiltonians	ergodic (satisfy ETH)
Performance time	$O(\beta n^3/\epsilon^2\Delta^3)$
Min # of ancilla	$O(\beta n^2/\epsilon\Delta)$
Min depth	$O(n^{o(1)}(\beta n^3/\epsilon^2\Delta^3)^{1+o(1)})$

The number of gates required is for the optimal trotterized decomposition of the Hamiltonian for lattice systems evolution using product formulas [56].

H. Details of simulations

Let us outline the details of the numerical simulations presented in Fig.2. In these simulations, we consider a one-dimensional architecture where we use a single ancilla per system qubit. We choose the local coupling operator in Eq.(2) as $V_{km} = a_{km}X_{s(m)} + b_{km}Z_{s(m)}$, where $s(m)$ is the index of the system qubit coupled to the mth ancilla qubit and $a_{km}, b_{km} \in \mathcal{N}(0,1)$ are generated from a normal distribution. We simulate the action of d maps in Eq. (S.2), where the expectation is taken over parameters $\{t_k, \omega_{km}, a_{mk}, b_{mk}\}$ and U_k are defined in Eq. (S.3). The probability of sampling eigenstate μ and the output energy are

$$p_\mu = \langle\mu|\mathbb{E}[\rho_d]|\mu\rangle, \quad E = \mathrm{Tr}\left(H\mathbb{E}[\rho_d]\right). \tag{S.90}$$

In order to simulate the noisy dynamics, we consider the dynamics

$$\rho_d^{\text{noisy}} = \mathbb{E}\,\mathcal{E}_d^{\text{noisy}} \circ \cdots \circ \mathcal{E}_1^{\text{noisy}}(\rho_0), \tag{S.91}$$

where, we the noisy cycles are modeled by the map

$$\mathcal{E}_k^{\text{noisy}} := \mathcal{D}_n \circ \cdots \circ \mathcal{D}_1 \circ \mathcal{E}_k \tag{S.92}$$

where $\mathcal{D}_m$ is single-qubit depolarizing channel acting on qubit m. It has the form

$$\mathcal{D}_m(\rho) = (1-3p)\rho + p\Big(X_m\rho X_m + Y_m\rho Y_m + Z_m\rho Z_m\Big), \tag{S.93}$$

where p is the error probability, X_m, Y_m and Z_m are Pauli matrices acting on system qubit m.

II. DETAILS OF UNIVERSAL ALGORITHM

In this section, we examine the universal algorithm in greater detail and analyze its convergence.

A. Description and regime

This algorithm consists of the following steps:

1. Initialize the system qubits in a random product state;
2. Set the ancilla qubits in the state $|0\rangle$;
3. Apply a cycle consisting of random gates to the system and ancilla qubits and measure the ancilla;
4. If at least one ancilla returns 1, reject the output and re-run the circuit. Otherwise, repeat step 2 if the number of completed cycles is smaller than d;
5. Measure the output.

There are three ways (modes) to implement the algorithm, depending on how we re-run the circuit. These modes are illustrated in Fig. S1.

In the first mode, the circuit is randomized every time we run it, regardless of whether the circuit is accepted or rejected. This allows us to obtain the average outcome. The resulting distribution is described by a circuit-averaged density matrix

$$\mathbb{E}[\rho_{\text{out}}] = \mathbb{E}_\theta[P(\boldsymbol{\theta})\rho_{\text{out}}(\boldsymbol{\theta})]/\mathbb{E}_\theta[P(\boldsymbol{\theta})], \tag{S.94}$$

where $\rho_{\text{out}}(\boldsymbol{\theta})$ is the accepted output state and $P(\boldsymbol{\theta})$ is probability of accepting the circuit, and the expectation is taken with respect to the random angles $\boldsymbol{\theta} = \{\theta_{km}\}$. In the second mode, the circuit is only randomized if it is accepted. In this way, we obtain the distribution of accepted outcomes described by a conditionally averaged

density matrix $\rho_{\text{out}} = \mathbb{E}_\theta \rho_{\text{out}}(\boldsymbol{\theta})$. In the third mode, the circuit is not randomized at all, except the first round. In this way, we obtain the distribution of outcomes for a fixed circuit. The resulting distribution is described by the density matrix $\rho_{\text{out}}(\boldsymbol{\theta})$.

The convergence of the algorithm is described by Theorem 2 in the main text, as well as in the extended Theorem S2 below. In particular, Theorem 2 describes the algorithm's performance for mode 1 and mode 3. The second mode is described in Theorem S2, which also describes all three cases together.

This work utilizes all three modes of the algorithm. For example, the averaged simulated curves in Fig. 2(a,b) in the main text are computed using mode 1. The optimized curves on the same plots, however, require the use of fixed gate angles throughout the experiment, which is equivalent to mode 3. Finally, IBMQ experiments are conducted using mode 2 because it requires fewer communication rounds with the device. Below, we analyze the performance of all three modes.

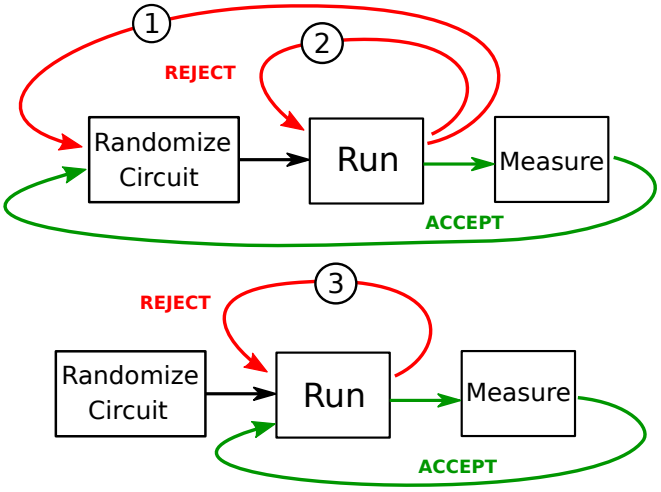


FIG. S1. **Modes of operation for the universal algorithm**. In mode 1, the circuit is randomized each time it is run. In mode 2, we run the same circuit a fixed number of times and randomize only after success. In mode 3, the circuit is randomly selected at the beginning of the experiment and remains fixed for the duration of the experiment.

B. Undivided Hamiltonian ($M = 1$)

Let us first consider a non-trotterized version of this algorithm that can be applied to arbitrary, non-local Hamiltonians. This case is equivalent to the number of ancilla being $M = 1$, when the Hamiltonian has only a single (global) term. In the section below, we will obtain a more general result for $M > 1$. For simplicity, we will focus on mode 1 here.

We begin by initializing the system in a random state on the n qubits, and the single-qubit ancilla to $|0\rangle$. To implement the algorithm, we apply a circuit containing d non-local $(n+1)$-qubit unitary gates defined by

$$U(\theta_k, H) := \exp\Big(i\theta_k \sqrt{\beta H/d} \otimes X\Big), \tag{S.95}$$

where $\theta_k \in \mathcal{N}(0,1)$ are independent Gaussian random variables, the Pauli operator X acts on the ancilla qubit, and the Hamiltonian H acts on the remaining n system qubits. We omitted index m for brevity as we have only one global n-qubit gate in this case. After each layer, we measure the ancilla qubit, reset it, and proceed to the next layer if the measurement returns zero. If the measurement returns a non-zero value, we repeat the circuit, resetting the values of θ_k before retrying.

Let us set the initial state of the system and ancilla qubit as $|\Psi_0\rangle = |\mathbf{z}\rangle \otimes |0\rangle$, where $|\mathbf{z}\rangle = |z_1, \ldots, z_n\rangle$ is a random initial state of the system and z_i are computational basis states, $z_i \in \{0, 1\}$. Then, the first global gate returns the state

$$\begin{aligned} U(\theta_1, H)|\Psi_0\rangle = &\cos\big(\theta_1\sqrt{\beta H/d}\big)|\mathbf{z}\rangle \otimes |0\rangle \\ &+ i\sin\big(\theta_1\sqrt{\beta H/d}\big)|\mathbf{z}\rangle \otimes |1\rangle. \end{aligned} \tag{S.96}$$

Let us define $\mathbb{E}[\rho_k]$ as the expected output after applying k gates and accepted measurements, including averaging over the initial states. After first gate, it has the form

$$\begin{aligned} \mathbb{E}[\rho_1] &\propto \mathbb{E}_{\theta_1,\mathbf{z}} \mathrm{Tr}_a \Big\{ I_{\text{sys}} \otimes |0\rangle\langle 0|U(\theta_1, H)|\Psi_0\rangle\langle\Psi_0|U^\dagger(\theta_1, H)\Big\} \\ &= \frac{1}{2^n}\mathbb{E}_{\theta_1} \cos^2(\theta_1\sqrt{\beta H/d}) \\ &= \frac{1}{2^{n+1}}\mathbb{E}_{\theta_1}\Big(I_{\text{sys}} + \cos(2\theta_1\sqrt{\beta H/d})\Big) \\ &= \frac{1}{2^{n+1}}\Big(I_{\text{sys}} + \exp(-2\beta H/d)\Big). \end{aligned} \tag{S.97}$$

As a result of repeating this procedure, it is straightforward to show that d-cycle algorithm returns the expected state

$$\mathbb{E}[\rho_{\text{out}}] \equiv \mathbb{E}[\rho_d] \propto \frac{1}{2^{n+d}}\Big(I + \exp(-2\beta H/d)\Big)^d. \tag{S.98}$$

Upon normalization, and using the binomial theorem, we obtain

$$\mathbb{E}[\rho_{\text{out}}] = \frac{1}{\mathcal{Z}_{\beta,d}} \sum_{k=0}^{d} \binom{d}{k} \exp(-\beta_k H), \tag{S.99}$$

where $\beta_k = 2\beta k/d$ is discrete inverse temperature, and $\mathcal{Z}_{\beta,d} = \mathrm{Tr}\,[e^{-\beta H}\cosh^d(\beta H/d)]$ is a modified partition function. In the limit of $d \to \infty$, the distribution over β_k asymptotically approaches to the singular value at inverse temperature β.

To evaluate the performance at finite but large d, we evaluate the distance between the quasi-thermal distribution in Eq.(S.99) and the Gibbs state by taking into account only the leading terms in the small parameter

$d^{-1} \ll 1$. In particular, we express

$$\begin{aligned}\rho_d &\propto \exp(-\beta H)\cosh^d(\beta H/d) \\ &= \exp\Big(-\beta H + \frac{\beta^2 H^2}{2d} + O\left(d^{-2}\right)\Big).\end{aligned} \tag{S.100}$$

Next, we establish the distance between this state and the Gibbs state by utilizing the following Lemma.

Lemma S4 *Consider Gibbs states*

$$\rho_\beta = \frac{1}{\mathcal{Z}_\beta} e^{-\beta H}, \quad \rho'_\beta = \frac{1}{\mathcal{Z}'_\beta} e^{-\beta(H+\lambda V)}, \tag{S.101}$$

where $\mathcal{Z}_\beta = \mathrm{Tr}\{e^{-\beta H}\}$, $\mathcal{Z}'_\beta = \mathrm{Tr}\{e^{-\beta(H+\lambda V)}\}$, H *and* V *are Hermitian operators, and* $\lambda \ll 1$ *is a small parameter. Then*

$$S\left(\rho_\beta \| \rho'_\beta\right) \le \frac{1}{2}\lambda^2\beta^2\Big(\langle V^2\rangle_\beta - \langle V\rangle_\beta^2\Big) + O(\lambda^3), \tag{S.102}$$

where $S(\cdot||\cdot)$ *is the relative entropy.*

Proof of Lemma S4. We can express the distance between Eq. (S.101) using the definition of relative entropy as

$$\begin{aligned}S\left(\rho_\beta \| \rho'_\beta\right) &:= \mathrm{Tr}\left(\rho_\beta(\log\rho_\beta - \log\rho'_\beta)\right) = \langle \log\rho_\beta - \log\rho'_\beta\rangle_\beta \\ &= -\log\mathcal{Z}_\beta + \lambda\beta\langle V\rangle_\beta + \log[\mathrm{Tr}\, e^{-\beta(H+\lambda V)}].\end{aligned} \tag{S.103}$$

By applying the Golden-Thompson inequality to the last term of this expression, we obtain

$$\begin{aligned}S\left(\rho_\beta \| \rho'_\beta\right) &\le \lambda\beta\langle V\rangle_\beta + \log \mathcal{Z}^{-1}\mathrm{Tr}\, e^{-\beta H}e^{-\lambda\beta V} \\ &= \lambda\beta\langle V\rangle_\beta + \log\langle e^{-\lambda\beta V}\rangle_\beta.\end{aligned} \tag{S.104}$$

Lastly, we utilize the Taylor series expansion to expand the last term of the previous equation as

$$\log\langle e^{-\lambda\beta V}\rangle_\beta = -\lambda\beta\langle V\rangle_\beta + \frac{1}{2}\lambda^2\beta^2\Big(\langle V^2\rangle_\beta - \langle V\rangle_\beta^2\Big) + O(\lambda^3). \tag{S.105}$$

By inserting this expansion into Eq. (S.104), we arrive at the statement of the Lemma. □

Using Eq. (S.100) and Lemma 1, where we set $\lambda \sim d^{-1}$ and $V = \beta^2 H^2/2 + O(d^{-1})$, we get

$$S(\rho_\beta \| \mathbb{E}[\rho_{\mathrm{out}}]) \le \frac{\beta^4}{8d^2}\Big(\langle H^4\rangle_\beta - \langle H^2\rangle_\beta^2\Big) + O\left(d^{-3}\right). \tag{S.106}$$

For physical local many-body Hamiltonians, the variance of the operator H^2 satisfies $\mathrm{Var}_\beta(H^2) = O(n^2)$, where n is the number of qubits. Therefore, the algorithm converges if the number of iterations d is of the order $d = O(\beta n)$.

C. Divided Hamiltonian ($M > 1$)

Let us prove a more general theorem that formalizes Theorem 2 in the main text. In our statement, we will specify the specific algorithm mode that produces the output for each quantity.

Theorem S2 (formal of Theorem 2) *Conisder Hamiltonian* $H = \sum_{m=1}^M h_m$ *and let* $\xi := \beta^2 M/d < 1$ *be small. Define* $A := \|h\|^2/4 + O(\xi)$ *for* $h := M^{-1}\sum_{m=1}^M h_m^2$ *and* $C := M^{-1}\sum_{m=1}^M \mathrm{Var}_\beta(h_m)\big(1 + O(\xi)\big)$. *Then for any* $0 < \epsilon \le 1$, *the output of Algorithm 1 after* d *cycles satisfies*

$$\textit{mode 1:} \quad S(\rho_\beta \,\|\, \mathbb{E}[\rho_{\mathrm{out}}]) \le A\xi^2\,, \tag{S.107}$$

$$\textit{mode 2:} \quad S(\rho_\beta \,\|\, \mathbb{E}_{\boldsymbol{\theta}}[\rho_{\mathrm{out}}(\boldsymbol{\theta})]) \le C\xi\,, \tag{S.108}$$

$$\textit{mode 3:} \quad \mathrm{Prob}\Big(S(\rho_\beta \,\|\, \rho_{\mathrm{out}}(\boldsymbol{\theta})) \ge \frac{\xi C}{\epsilon}\Big) \le \epsilon\,, \tag{S.109}$$

where $S(\rho\|\sigma)$ *is the relative entropy and the expectation* $\mathbb{E}[\rho_{\mathrm{out}}]$ *is defined in Eq.* (S.94).

We recall that the system state dynamics includes d cycles, each consisting of M gates in Eq. (4), followed by postselected measurements of the ancilla. Let $\rho_{km}(\boldsymbol{\theta})$ be the state of the system qubits after the measurement of the m-th gate in the k-th cycle, where $\boldsymbol{\theta} := \{\theta_{km}\}$ denotes the set of gate angles. We define $P_{km}(\boldsymbol{\theta})$ to be the probability of acceptance of the overall circuit at this stage, i.e., that all ancillas up to this point are measured in the zero state. We then define $r_{km}(\boldsymbol{\theta}) := P_{km}(\boldsymbol{\theta})\rho_{km}(\boldsymbol{\theta})$, which for $m \ge 2$ and a given cycle k, can be written as

$$\begin{aligned}r_{km}(\boldsymbol{\theta}) &= P_{k,m-1}(\boldsymbol{\theta})\times \\ &\quad \mathrm{Tr}_a\Big\{I_{\mathrm{sys}} \otimes |0\rangle\langle 0| U_{km}\Big(\rho_{k,m-1}(\boldsymbol{\theta}) \otimes |0\rangle\langle 0|\Big)U_{km}^\dagger\Big\} \\ &\quad = \Phi_m(r_{k,m-1}(\boldsymbol{\theta}))\end{aligned} \tag{S.110}$$

where $U_{km} := U(\theta_{km}, h_m)$ is defined in Eq. (4) in the main text and we defined the linear map

$$\Phi_m(\rho) := \cos(\theta_{km}\sqrt{\beta h_m/d})\,\rho\,\cos(\theta_{km}\sqrt{\beta h_m/d}). \tag{S.111}$$

Using this recurrence relation, we can also connect the probability-weighted state of the system at the end of the $k-1$st cycle to the one at the beginning of the kth cycle

$$r_{kM}(\boldsymbol{\theta}) = \Phi_M \circ \Phi_{M-1} \circ \cdots \circ \Phi_1(r_{k-1,M}) \tag{S.112}$$

where $\mathcal{A}\circ\mathcal{B}(\rho) = \mathcal{A}(\mathcal{B}(\rho))$ is the composition of channels A and B.

We set the input state to be the fully mixed state, i.e. $\rho_0 = I/2^n$, where I is $2^n \times 2^n$ identity matrix. Then, the overall circuit output is

$$P_{M,d}(\boldsymbol{\theta})\rho_{M,d}(\boldsymbol{\theta}) = \mathcal{C}(\boldsymbol{\theta})\rho_0\mathcal{C}^\dagger(\boldsymbol{\theta}) = \frac{1}{2^n}\mathcal{C}(\boldsymbol{\theta})\mathcal{C}^\dagger(\boldsymbol{\theta}), \tag{S.113}$$

where we defined the propagator

$$\mathcal{C}(\boldsymbol{\theta}) := \prod_{k=1}^{d}\Big(\prod_{m=1}^{M}\cos\theta_{km}\sqrt{\beta h_m/d}\Big). \tag{S.114}$$

and $\prod_{m=1}^{M}$ is ordered direct product defined as $\prod_{m=1}^{M} a_m := a_M \dots a_1$. The asymptotic behaviour of the output state in Eq. (S.113) is given by the following Lemma.

Lemma S5 *Assuming that d^{-1} is small, then*

$$\mathcal{C}(\boldsymbol{\theta})\mathcal{C}^\dagger(\boldsymbol{\theta}) = \exp\Big[-\beta\Big(H+\frac{1}{d}V\Big)\Big], \tag{S.115}$$

where

$$V = \sum_{m=1}^{M}\sum_{k=1}^{d}\Big[(\theta_{km}^2-1)h_m + \frac{\beta}{6d}\theta_{km}^4 h_m^2\Big] + O(1). \tag{S.116}$$

Proof of Lemma S5. First, we use Taylor's expansion by inverse depth d^{-1} to express

$$\begin{aligned}\cos\theta_{km}\sqrt{\beta h_m/d} &= 1 - \frac{\beta h_m}{2d}\theta_{km}^2 + \frac{\beta^2 h_m^2}{24d^2}\theta_{km}^4 + O\Big(\frac{1}{d^3}\Big)\\ &= \exp\left[-\frac{\beta h_m}{2d}\theta_{km}^2 - \frac{\beta^2 h_{mk}^2}{12d^2}\theta_{km}^4 + O\Big(\frac{1}{d^3}\Big)\right]\\ &= \exp\Big(-\frac{\xi_{mk}}{2d}\Big),\end{aligned} \tag{S.117}$$

where $\xi_{mk} := \beta\theta_{km}^2 h_m + \beta^2\theta_{km}^4 h_{mk}^2/6d + O(d^{-2})$. Using this representation, we rewrite

$$\mathcal{C}(\boldsymbol{\theta})\mathcal{C}^\dagger(\boldsymbol{\theta}) = \mathcal{E}(\boldsymbol{\theta})\mathcal{E}^\dagger(\boldsymbol{\theta}). \tag{S.118}$$

where

$$\mathcal{E}(\boldsymbol{\theta}) := \prod_{k=1}^{d}\prod_{m=1}^{M}\exp\Big(-\frac{\xi_{mk}}{2d}\Big). \tag{S.119}$$

Using second-order Suzuki-Trotter product formula (see [49, 56]), we express

$$\mathcal{E}(\boldsymbol{\theta})\mathcal{E}^\dagger(\boldsymbol{\theta}) = \exp\Big(-\frac{1}{d}\sum_{m=1}^{M}\sum_{k=1}^{d}\xi_{mk} + O\Big(\frac{1}{d^2}\Big)\Big). \tag{S.120}$$

Using this result, we obtain the expression

$$\begin{aligned}&\mathcal{C}(\boldsymbol{\theta})\mathcal{C}^\dagger(\boldsymbol{\theta}) =\\ &= \exp\Big(-\frac{\beta}{d}\sum_{m=1}^{M}\sum_{k=1}^{d}\Big\{\theta_{km}^2 h_m + \frac{\beta}{6d}\theta_{km}^4 h_m^2\Big\} + O\Big(\frac{1}{d^2}\Big)\Big)\\ &= \exp\Big(-\beta H - \frac{\beta}{d}\sum_{m=1}^{M}\sum_{k=1}^{d}\Big\{(\theta_{km}^2-1)h_m\\ &\qquad + \frac{\beta}{6d}\theta_{km}^4 h_m^2\Big\} + O\Big(\frac{1}{d^2}\Big)\Big).\end{aligned} \tag{S.121}$$

This leads us to the statement of the Lemma. □

Next, let us derive the performance bounds of the algorithm in mode 1. For this purpose, we first express the expected density matrix as

$$\mathbb{E}[\rho_{\rm out}] = \mathbb{E}_{\boldsymbol{\theta}}\mathcal{C}(\boldsymbol{\theta})\mathcal{C}^\dagger(\boldsymbol{\theta})/\mathrm{Tr}\left(\mathbb{E}_{\boldsymbol{\theta}}\mathcal{C}(\boldsymbol{\theta})\mathcal{C}^\dagger(\boldsymbol{\theta})\right) \tag{S.122}$$

Using Lemma S5, we get

$$\begin{aligned}S(\rho_\beta\|\mathbb{E}[\rho_{\rm out}]) &= \langle\rho_\beta - \mathbb{E}[\rho_{\rm out}]\rangle_\beta\\ &= -\log\mathcal{Z}_\beta - \beta H + \log\mathbb{E}_{\boldsymbol{\theta}}\mathrm{Tr}\,e^{-\beta(H+V/d)}\\ &\quad - \langle\log\mathbb{E}_{\boldsymbol{\theta}}e^{-\beta(H+V/d)}\rangle_\beta\end{aligned} \tag{S.123}$$

where the operator V is defined in Lemma S5. In order to evaluate this expression, we rewrite the exponent as

$$\exp(-\beta H - \beta V/d) = \exp(-\beta H)\exp(-\beta\varphi(V)/d), \tag{S.124}$$

where we introduced the linear transformation

$$\varphi(O) := \int_0^1 d\tau e^{\tau H} O e^{-\tau H}. \tag{S.125}$$

Based on the decomposition in Eq. (S.124), we can rewrite relative entropy as

$$S(\rho_\beta\|\rho_{\beta,d}) = \log\mathbb{E}_{\boldsymbol{\theta}}\langle e^{-\beta\varphi(V)}\rangle_\beta - \langle\log\mathbb{E}_{\boldsymbol{\theta}}e^{-\beta\varphi(V)}\rangle_\beta. \tag{S.126}$$

Next, we evaluate the leading order contribution using Taylor expansion as

$$S(\rho_\beta\|\rho_{\beta,d}) = \frac{1}{2d^2}\Big(\langle[\mathbb{E}_{\boldsymbol{\theta}}\varphi(V)]^2\rangle_\beta - \langle\mathbb{E}_{\boldsymbol{\theta}}\varphi(V)\rangle_\beta^2\Big) + O(d^{-3}). \tag{S.127}$$

The expectation over the gate angles is

$$\mathbb{E}_{\boldsymbol{\theta}}\varphi(V) = \frac{\beta^2}{2d}\varphi(h) + O(d^{-3}), \tag{S.128}$$

where we use the notation

$$h := \frac{1}{M}\sum_{m=1}^{M} h_m^2. \tag{S.129}$$

Using the property $\langle\varphi(O)\rangle_\beta = \langle O\rangle_\beta$, we finally express

$$S(\rho_\beta\|\rho_{\beta,d}) = \frac{\beta^4 M^2}{8d^2}\Big(\langle\varphi(h)^2\rangle_\beta - \langle h\rangle_\beta^2\Big) + O(d^{-3}). \tag{S.130}$$

This formula is a generalization of Eq. (S.106). Because the transformation in Eq. (S.125) does not change the spectral norm of the operator, we can bound the expression as

$$S(\rho_\beta\|\rho_{\beta,d}) \le A\frac{\beta^4 M^2}{d^2}. \tag{S.131}$$

where $A = \|h\|^2/4 + O(d^{-1})$. Assuming that the norm $\|h_m\| \le O(1)$ is finite, parameter A is also constant, $A \sim O(1)$.

Next, to derive the bounds for modes 2 and 3, we combine Lemmas S4 and S5 to express

$$\mathbb{E}_{\boldsymbol{\theta}} S(\rho_\beta \| \rho(\boldsymbol{\theta})) \leq \frac{\beta^2}{2d^2} \mathbb{E}_{\boldsymbol{\theta}} \Big(\langle V^2 \rangle_\beta - \langle V \rangle_\beta^2 \Big) + O(d^{-3}). \tag{S.132}$$

We obtain

$$\mathbb{E}_{\boldsymbol{\theta}} \langle V \rangle_\beta^2 = 2d \sum_{m=1}^{M} \langle h_m \rangle_\beta^2 + O(1). \tag{S.133}$$

Therefore, the expected relative entropy is

$$\mathbb{E}_{\boldsymbol{\theta}} S(\rho_\beta \| \rho(\boldsymbol{\theta})) \leq \frac{C\beta^2 M}{d}, \tag{S.134}$$

where we denoted

$$C = \frac{1}{M} \sum_{m=1}^{M} \mathrm{Var}_\beta(h_m) + O(d^{-1}). \tag{S.135}$$

where $\mathrm{Var}_\beta(x) = \langle x^2 \rangle_\beta - \langle x \rangle_\beta^2$.

By Jensen's inequality, we have

$$S(\rho_\beta \| \mathbb{E}[\rho_{\beta,d}]) \leq \mathbb{E} S(\rho_\beta \| \rho_{\beta,d}) \leq \frac{C\beta^2 M}{d}. \tag{S.136}$$

Using Markov's inequality, for any $x > 0$ we have

$$\mathrm{Prob}\Big(S(\rho_\beta \| \rho(\boldsymbol{\theta})) \geq x \Big) \leq \frac{1}{x} \mathbb{E}_{\boldsymbol{\theta}} S(\rho_\beta \| \rho(\boldsymbol{\theta})). \tag{S.137}$$

Using Eq. (S.134) and choosing $x = \mathbb{E}_{\boldsymbol{\theta}} S(\rho_\beta \| \rho(\boldsymbol{\theta}))/\epsilon$, we obtain the expression

$$\mathrm{Prob}\Big(S(\rho_\beta \| \rho(\boldsymbol{\theta})) \geq \frac{C\beta^2 M}{\epsilon d} \Big) \leq \epsilon. \tag{S.138}$$

Thus, we prove Theorem 1.

D. Success probability

Our final goal is to derive the acceptance probability, i.e. the probability that all the ancilla measurements return zero. The probability of such event success is given by (S.113) as

$$\begin{aligned} p \equiv P_{M,d}(\boldsymbol{\theta}) &= \frac{1}{2^n} \mathbb{E}_{\boldsymbol{\theta}} \mathrm{Tr}\, \mathcal{C}(\boldsymbol{\theta}) \mathcal{C}^\dagger(\boldsymbol{\theta}) \\ &= 2^{-n} \mathrm{Tr}\, e^{-\beta H} + O(d^{-1}) \end{aligned} \tag{S.139}$$

Therefore, for large-d circuits

$$P \simeq 2^{-\alpha n}, \quad \alpha = 1 - (\log_2 \mathcal{Z}_\beta)/n \tag{S.140}$$

Note that $\beta = 0$ corresponds to the partition function $\mathcal{Z}_\beta = 2^n$ for any Hamiltonian. In this case the success probability is $P_d = 1$. This observation is easily explained by noting that in the case $\beta = 0$ all the gates in the circuit are trivial and the system state is already initialized in infinite-temperature (fully mixed) state.

E. Resource estimation

In this section, we provide a summary of the resources required for implementing the algorithm. As in the main text, n is the number of qubits for the target Hamiltonian, β is the inverse temperature, and ϵ is the algorithm's error.

Type of Hamiltonians	any
Performance time	$2^{\Theta(n)}$
Min # of ancilla	1
Min depth	$O(\beta^2 n^2/\epsilon)$ (generic) $O(\beta^2 n^2/\sqrt{\epsilon})$(average)

We provide the number of gates both for the circuit-averaged sampling and for a generic circuit outcome.

F. Details of simulation

We simulate the *accepted* output state using the expression

$$\rho_{\mathrm{out}}(\boldsymbol{\theta}) = \frac{1}{P(\boldsymbol{\theta})} \mathcal{E}'_d \circ \cdots \circ \mathcal{E}'_1(\rho_0), \tag{S.141}$$

where ρ_0 is the initial fully mixed state of the system qubits, $\boldsymbol{\theta} = \{\theta_{km}\}$ are gate angles, and $P(\boldsymbol{\theta})$ is the probability of accepting the circuit,

$$P(\boldsymbol{\theta}) = \mathrm{Tr}\, \mathcal{E}'_d \circ \cdots \circ \mathcal{E}'_1(\rho_0). \tag{S.142}$$

The channels $\mathcal{E}'_k$ represent the transformation of the system qubits during the corresponding algorithm cycle. Such channels are the composition of channels generated by each gate in Eq. (4) and corresponding ancilla measurement, i.e.

$$\mathcal{E}'_k = \mathcal{E}'_{kM} \circ \cdots \circ \mathcal{E}'_{k1}, \tag{S.143}$$

where

$$\mathcal{E}'_{km}(\rho) := \mathrm{Tr}_a \Big\{ (I_{\mathrm{sys}} \otimes |0\rangle\langle 0|) U_{km} \big(\rho \otimes |0\rangle\langle 0| \big) U_{km}^\dagger \Big\}, \tag{S.144}$$

$U_{km} = U(\theta_{km}, h_m)$, and $|0\rangle$ represents the initial state of the ancilla qubit. The probability of sampling the eigenstate of the Hamiltonian is given by the formula

$$n_\mu = \mathbb{E}_{\boldsymbol{\theta}} P(\boldsymbol{\theta}) \langle \mu | \rho_{\mathrm{out}}(\boldsymbol{\theta}) | \mu \rangle / \mathbb{E}_{\boldsymbol{\theta}} P(\boldsymbol{\theta}), \tag{S.145}$$

where $|\mu\rangle$ are eigenstates of the Hamiltonian. The result is shown in Fig. 2(a) right panel (blue circled lines) for $\beta = 1$ compared to the theoretical prediction (dashed line)

$$n_\mu^{\mathrm{theor}} = \mathcal{Z}^{-1} \exp(-\beta E_\mu), \quad \mathcal{Z} = \sum_\mu \exp(-\beta E_\mu). \tag{S.146}$$

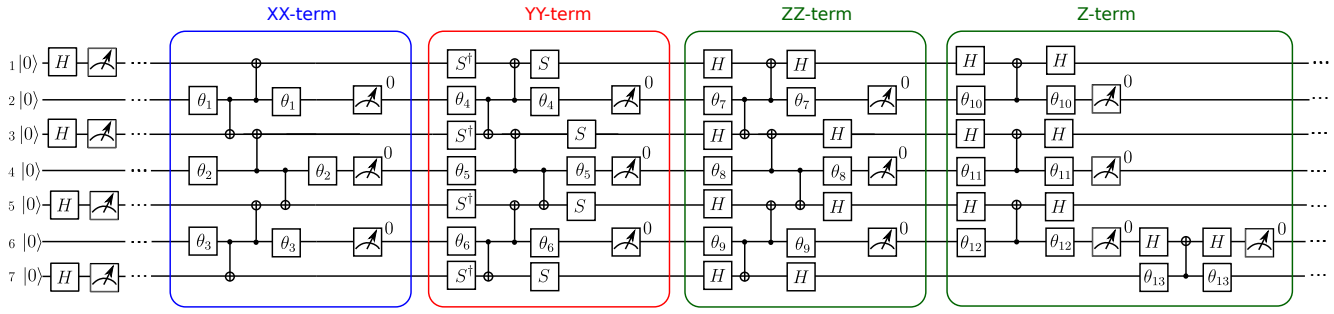


FIG. S2. **Universal algorithm with native gates**. The circuit for the universal algorithm contains d identical cycles; here we show only one cycle. In each cycle, three sub-cycles implement the terms XX, YY, ZZ, and Z, according to the decomposition in Eqs. (S.151) and (S.152). Gates labeled H and S denote Hadamard gates and standard S gates, gates labeled θ_k (here we have omitted the cycle label) implement unitaries $u_{km} = \exp(\frac{1}{2} i\theta_k v_m X)$, $v_m = \sqrt{\beta\alpha_m/d}$, α_m is the coefficient if front of the Hamiltonian Pauli term, and the symbol "0" next to a box indicates a postselected measurement.

We also evaluate the temperature dependence of the output energy

$$E = \mathbb{E}_{\boldsymbol{\theta}} P(\boldsymbol{\theta}) \mathrm{Tr}\left(\rho_{\mathrm{out}}(\boldsymbol{\theta}) H\right) / \mathbb{E}_{\boldsymbol{\theta}} P(\boldsymbol{\theta}), \tag{S.147}$$

and compare it to theoretical thermal value,

$$E_{\mathrm{theor}} = \sum_{\mu} E_{\mu} \exp(-\beta E_{\mu}). \tag{S.148}$$

The output energy dependence is shown in Fig. 2(b) right panel by blue line (circles) and the thermal value is depicted by dashed line.

To consider the effect of noise, we replace the channels in Eqs. (S.141) and Eq. (S.142) by

$$\mathcal{E}'_{km} \to \mathcal{E}'^{\mathrm{noisy}}_{km} := \mathcal{D}_{mi_q} \circ \cdots \circ \mathcal{D}_{mi_1} \circ \mathcal{E}'_{km} \tag{S.149}$$

where $i_1 \ldots i_q$ enumerate the qubits on which U_{km} is acting, and we defined single-qubit depolarizing channel as

$$\mathcal{D}_{mi}(\rho) = (1 - 3p_m)\rho + p_m \Big(X_i \rho X_i + Y_i \rho Y_i + Z_i \rho Z_i \Big), \tag{S.150}$$

X_i, Y_i, and Z_i are Pauli operators acting on qubit i, and p_m is the depolarizing error probability for gate m. The error probability is determined by the gate's structure. We demonstrate below that any two-qubit U_{km} for Hamiltonian Pauli terms can be decomposed using single-qubit gates and one two-qubit native gate (for example, CNOT). In addition, any such three-qubit gate U_{km} can be decomposed using two CNOTs. Given that the CNOTs contribute the majority of error, it is reasonable to assume that three-qubit gates will have twice the error of two-qubit gates for Pauli Hamiltonian terms. Fig. 2. Right panels of Figures (a) and (b) show the results of the noisy simulation as a green curve (diamonds)
.

G. Optimized implementation

The representation of generic gates as standard one- and two-qubit gates is resource-demanding. There is a way to represent a generic two-qubit gate using only three two-qubit entangling gates [50]. A generic three-qubit gate, however, would require many two-qubit entangling gates to be implemented.

In our case, there is a way to avoid similar computational burdens. As we recall, ancilla qubits are measured after every gate, and we accept circuits if the measurement is zero. Therefore, each two- or three-qubit gate has a zero ancilla value in its input. Then, in the case of this particular input and Pauli terms in Eq. (7), there is a simpler method of implementing desired circuits. Gates dedicated to the terms $h_m \propto Z_i$ can be implemented, for example, by just a single entangling gate

$$\begin{aligned} &\mathrm{R}_X(\theta)|\psi\rangle|0\rangle \equiv \\ &\quad \mathrm{R}_X(\theta) H_i \cdot \mathrm{CNOT}_{A\to i} \cdot H_i \mathrm{R}_X(\theta)\,|\psi\rangle|0\rangle, \end{aligned} \tag{S.151}$$

where H_i is Hadamard gate for qubit i, $\mathrm{CNOT}_{A\to i}$ is a controlled NOT gate that applies to qubit i and uses the ancilla A as control, and $\mathrm{R}_X(\theta) = \exp(\frac{1}{2} i\theta X_A)$ acts on ancilla qubit. Similarly, the gate implementing the term $h_m \propto X_i X_j$ requires only two controlled-NOT operations and single-qubit gates,

$$\begin{aligned} &\exp\Big(i\theta \frac{1}{2}(I + X_i X_j) X_A\Big)|\psi\rangle|0\rangle \equiv \\ &\quad \mathrm{R}_X(\theta)\,\mathrm{CNOT}_{A\to i}\,\mathrm{CNOT}_{A\to j}\,\mathrm{R}_X(\theta)|\psi\rangle|0\rangle, \\ &\exp\Big(i\theta \frac{1}{2}(I + Y_i Y_j) X_A\Big)|\psi\rangle|0\rangle \equiv \\ &\quad \mathrm{R}_X(\theta)\,S_i\,S_j\,\mathrm{CNOT}_{A\to i}\,\mathrm{CNOT}_{A\to j}\,S_i^\dagger\,S_j^\dagger\,\mathrm{R}_X(\theta)|\psi\rangle|0\rangle, \\ &\exp\Big(i\theta \frac{1}{2}(I + Z_i Z_j) X_A\Big)|\psi\rangle|0\rangle \equiv \\ &\quad \mathrm{R}_X(\theta)\,H_i\,H_j\,\mathrm{CNOT}_{A\to i}\,\mathrm{CNOT}_{A\to j}\,H_i\,H_j\,\mathrm{R}_X(\theta)|\psi\rangle|0\rangle, \end{aligned} \tag{S.152}$$

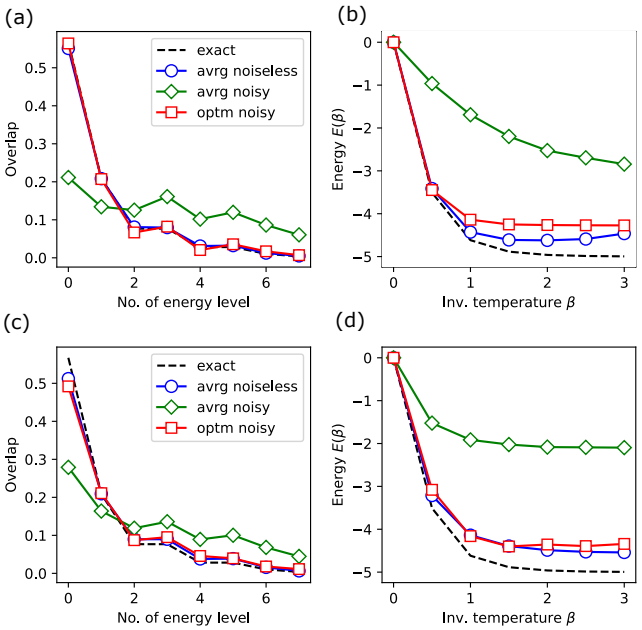


FIG. S3. **Additional simulations.** (a)-(b) Simulation results for universal algorithm utilizing $n_a = 2$ ancilla qubits for 3-qubit Hamiltonian in Eq. (S.155), $t = -2$, $U = 4$ and $h_i = -1$ (Heisenberg model). The inverse temperature is $\beta = 1$ and number of cycles is $d = 5$. Panel (a) shows the overlap between expected output state in Eq. (S.94) and the eigenstates of the Hamiltonian for noiseless circuit (blue circles), noisy circuit (green diamonds), noisy optimized circuit (red squares), and exact solution (dashed line). We use a depolarizing noise model with single-qubit error probability $p_2 = 0.01$ for 2-qubit gates and $p_3 = 0.02$ for 3-qubit gates. An averaged circuit output is computed for 10^3 successful sample runs. (b) Output state energy as a function of temperature for the same setting as the panel (a). (c)-(d) Performance for ergodic algorithm for the same setting as Panel (a)-(b), except using $d = 20$ cycles, $\gamma = 0.1$, and single-qubit depolarizing error probability $p = \Gamma t$ after each cycle, where t is the cycle time and $\Gamma = 10^{-3}$. The average is based on 10^3 sample runs.

where S_i is S-gate on ith qubit. The circuit for the Hamiltonian in Eq. (7) is shown in Fig. S2. As this circuit is built from native gates, its implementation is straightforward using tools such as IBM Qiskit.

III. MAPPING TO QUBITS

In the main text, we considered the hard-core boson model Hamiltonian, which is expressed as

$$H = -J \sum_{\langle i,j \rangle} \left(a_i^\dagger a_j + a_j^\dagger a_j \right) + U \sum_{\langle i,j \rangle} n_i n_j, \tag{S.153}$$

where a_i, $a_i^\dagger$ are hardcore-boso Fock operators that satisfy conditions $[a_j, a_j^\dagger] = 0$ for all $i \neq j$ and $\{a_i, a_i^\dagger\} = 1$ for the same site. These operators can be mapped to the qubit Pauli operators using the transformation

$$a_i = \frac{1}{2}(X_i - iY_i), \qquad a_i^\dagger = \frac{1}{2}(X_i + iY_i). \tag{S.154}$$

For the one-dimensional setting, we obtain the qubit Hamiltonian

$$\begin{aligned} H = -\frac{J}{2} \sum_{i=1}^{N-1} \left(X_i X_{i+1} + Y_i Y_{i+1} \right) \\ + \frac{U}{4} \sum_{i=1}^{N-1} Z_i Z_{i+1} + \sum_i h_i Z_i, \end{aligned} \tag{S.155}$$

where $h_i = -U/2$ for $j = 2, \ldots, N-1$ and $h_i = -U/4$ for $j = 1, N$. It is possible to generate the Gibbs state for this Hamiltonian using this one-dimensional circuit architecture. Some additional simulation data for the spin model in Eq. (S.155) are shown in Fig. S3.